energies

MDPI

Review

Recent Progress and Challenges in MXene-Based Phase Change Material for Solar and Thermal Energy Applications

Hafiz Taimoor Ahmed Awan [1], Laveet Kumar [2], Weng Pin Wong [1,3], Rashmi Walvekar [3,*] and Mohammad Khalid [1,4,5,*]

[1] Graphene & Advanced 2D Materials Research Group (GAMRG), School of Engineering and Technology, Sunway University, Petaling Jaya 47500, Malaysia
[2] Department of Mechanical Engineering, Mehran University of Engineering and Technology, Jamshoro 76062, Pakistan
[3] Department of Chemical Engineering, School of New Energy and Chemical Engineering, Xiamen University Malaysia, Sepang 43900, Malaysia
[4] Sunway Materials Smart Science & Engineering (SMS2E) Research Cluster, Sunway University, Petaling Jaya 47500, Malaysia
[5] School of Applied and Life Sciences, Uttaranchal University, Dehradun 248007, India
* Correspondence: rashmi.walvekar@xmu.edu.my (R.W.); khalids@sunway.edu.my (M.K.)

Abstract: Energy storage is becoming a critical issue due to the diminishing availability of fossil fuels and the intermittent nature of current renewable energy sources. As a result, thermal management (TM) and thermal energy systems have gained significant attention due to their crucial roles in various industries. Among the different TM materials, MXenes, a member of the transition metal carbide/nitride family, have emerged as a promising material due to their unique 2D nanostructure, changeable surface chemistry, high electrical/thermal conductivity, light absorptivity, and low infrared emissivity. This review outlines the synthesis methods of MXenes and their various features and applications in thermal management. These 2D materials exhibit outstanding optical and thermal properties, making them suitable for thermal energy generation and storage. The study also covers the potential applications of MXene in the desalination industry, hybrid photovoltaic thermal systems, solar energy storage, electronics, and other thermal management related industries. The findings suggest that MXene-based TM materials have remarkable features that significantly influence thermal energy storage and conversion and present opportunities for further research in efficiently using these materials.

Keywords: MXene; photovoltaic; phase change materials; solar energy; thermal management

Citation: Awan, H.T.A.; Kumar, L.; Wong, W.P.; Walvekar, R.; Khalid, M. Recent Progress and Challenges in MXene-Based Phase Change Material for Solar and Thermal Energy Applications. *Energies* **2023**, *16*, 1977. https://doi.org/10.3390/en16041977

Academic Editors: Emiliano Borri, Gabriel Zsembinszki and Marilena De Simone

Received: 13 January 2023
Revised: 6 February 2023
Accepted: 14 February 2023
Published: 16 February 2023

1. Introduction

Due to its significant role in numerous situations, including energy-saving cooling and heating [1], heat dissipation in electronic devices [2], fire/flame retardant in batteries [3], personal thermal management [4], waste heat recovery [5], thermotherapy [6], solar energy utilization [7], and thermal camouflage [8], the field of thermal management (TM) has developed quickly over the past 10 years. TM materials undoubtedly influence the management and usage efficiency of thermal energy. Numerous materials have been thoroughly investigated for TM, including metals [9], organic polymers [10], inorganic nonmetallic materials [11], semiconductors [12], and carbon nanotubes (CNTs) [13]. However, they still cannot match the stringent requirements of several temperature conditions. A lot of people around the world are interested in finding high-performance TM materials.

On the other hand, due to advances in energy storage and solar thermal energy harvesting over the past few decades, the use of solar energy is growing in our modern world to address environmental problems [14]. Numerous extensive investigations have been conducted to meet the energy requirements for effective operating systems [15]. This energy

can be conserved and harnessed through mechanical, thermal, and electrical techniques. The storage of thermal energy can be achieved through various methods, including sensible heat storage, latent heat storage, thermochemical storage, or a combination thereof. It has been established that using phase change materials (PCMs) in latent heat storage during phase transitions is an efficient way to conserve thermal energy. The results showed that the phase change materials are excellent for storing thermal energy and that their huge storage densities have sensible heat storage capacities that are 5–10 times greater [16,17].

Raymond researched PCMs as energy storage materials for the first time in 1940 [18], and following that, during the energy crisis of 1973–1974, PCMs were used as energy storage for thermal control [19]. The current scarcity of fossil fuels and the dangers of greenhouse gas emissions makes it essential to use energy wisely. The performance of home and commercial systems can be improved using these storage materials, which provide the best thermal storage and usage solution [20–22]. The energy storage capacity of sensible heat storage materials is inferior to that of latent heat storage materials. As a result, thermal energy can be stored and released effectively through phase changes without altering temperature. The phase change materials (PCMs) exhibit excellent heat absorption or release capabilities during phase transitions, making selecting an appropriate PCM a crucial factor in the process [23]. Organic and inorganic eutectic materials can be classified as phase change materials. Paraffin and non-paraffinic elements are present in the organic materials. There are several different non-paraffins, including esters, fatty acids, alcohol, and glycol. The inorganic materials include metals and alloys, salts, salt hydrates, and salt eutectic. As further discussed in the section, polyurethane and polybutadiene are among the solid–solid phase change media.

Therefore, to analyze the flow of fluid and the distribution of heat in a chilled water storage system, Selamat et al. [24] used a computational fluid dynamic technique. The investigation was conducted on three separate scenarios: the presence of a diffuser in a tank, the absence of a diffuser in a tank, and the presence of a diffuser without a tank. The findings of the research were consistent with the analytical data and served as validation for future studies. Additionally, Rashid [25] studied the effect of the presence or absence of phase transition material on the productivity of solar stills. As thermal energy storage for latent heat, polyvinyl pyrrolidone, polyethylene glycol, and sodium salt of carboxymethyl cellulose were applied. The studies were conducted throughout October, and it was discovered that employing PCM increased still productivity by 25 to 40% compared to not using PCM. Several improved energy storage materials have been created, such as molten salt nanofluids, composite PCMs (nano-based PCMs), cascade PCMs, and hybrid PCMs. These enhanced energy storage materials offer significantly improved thermal characteristics compared to conventional ones. Furthermore, the utilization of nano-enhanced heat transfer fluids, specifically binary molten salt nanofluids, has demonstrated the potential for further enhancement of collector efficiency, as illustrated in Figure 1a. Karishna et al. [26] described the various kinds of heat transfer fluids to enhance the effectiveness of the parabolic trough collector. The optimal temperature range for parabolic trough collector operation in power generation applications lies between 150 °C and 800 °C. However, the conventional method of thermal modification has proven to provide limited efficiency improvements, with a maximum increase of only 2%. The same group [27] also proposed the idea of a fatty acid/metal ion composite for energy storage applications. In an effort to enhance the thermophysical properties, sodium metal was blended with varying concentrations of lauric acid from 0.2, 0.5, and 1 weight percent. The results indicated that adding metal ions improved phase transition enthalpy compared to pure lauric acid. However, the decrease in melting temperature was lowered as the weight of metal ions increased.

Using the response surface approach, Asfattahi et al. [28] improved the heat conductivity of a nano PCM made of paraffin wax and graphene. The primary factor impacting the value of thermal conductivity was temperature. The value of "k" was predicted through general correlation. The optimal value of "k" was found to be 0.275 W/mK at a temperature of 69.73 °C and a mass fraction of 0.186 wt% graphene. The integration of these

materials significantly improved the value of thermal conductivity and energy storage capacity. However, there are still limitations in terms of thermal stability, storage capacity, and formation methodology that require further investigation. Selecting the appropriate phase change material (PCM) for the specific application is critical to maximizing stability and energy storage performance. Future research should address these limitations and identify the optimal PCM type.

Since the discovery of graphene in 2004, several 2D materials have been identified, including transition metals, oxides, and boron nitrides [29–31]. Due to its exceptional qualities, graphene has been widely used as a 2D material across various applications.

Later in 2011, Naguib et al. [32] selectively etched "A" elements, often referred to as MAX phases, to produce selective 2D materials. These 2D stacked MXene are comparable to graphene [33]. Additionally, the properties of MXene exhibit similarities to reduced graphene oxide (rGO) and graphene oxide (GO), including the ability to be modified through surface termination. Besides possessing hydrophilic and water-soluble qualities, the modulus of MXene is also twice that of rGO and GO. It also demonstrates superior electrical conductivity, 5.0–10.0 times more conductive than rGO, and greater transparency in the visible light range. Besides, MXene-based phase change materials have been identified as novel players in the field of thermal management, displaying remarkable thermal performance characteristics. The ongoing investigation of these materials has initiated a paradigm shift in thermal management, with MXene being the preferred material due to its superior electrical conductivity, mechanical robustness, and optical transparency in thin films. The easily tunable properties through composition and structure, as well as its efficient light-to-heat conversion, are the key features that make MXene a valuable material for thermal management applications.

Parashar et al. [34] used the artificial neural network (ANN) to predict the dynamic viscosity of MXene palm oil nanofluids. They measured the dynamic viscosity across a broad temperature range of 18 to 100 °C. It was discovered that temperature significantly impacts dynamic viscosity, which also decreases with rising temperatures. The artificial neural network model was also developed using temperature and concentration as input parameters and dynamic viscosity as output parameters. The model and experimental data were in good agreement, and a 95.67% error was found to be within 2%, as shown in Figure 1b. Similarly, Aslfattahi et al. [35] examined the silicon oil-based MXene nanofluids in concentrated photovoltaic thermal systems at three different concentrations. Upon reaching maximum concentration, a 64% increase in the "k" value was observed. However, no variations in viscosity were detected with the addition of nanoparticles. Further evaluations of thermal conductivity and viscosity were conducted, and the results indicated that silicon oil-based MXene nanofluids enhanced the cooling performance of photovoltaic systems. The cooling efficacy was found to be directly proportional to the concentration of the nanoparticles.

This review presents an overview of the synthesis methods for MXenes and an examination of the distinctive characteristics of these 2D materials and their composites. A particular focus is placed on the thermal engineering applications of MXene, including the utilization of MXene-based phase transition materials for nanofluid applications. The outcomes of these applications are noteworthy and demonstrate the potential for further exploration in the field of thermal management. These findings will serve as a valuable resource for future research in this area, providing a foundation for further investigation and advancements in thermal management.

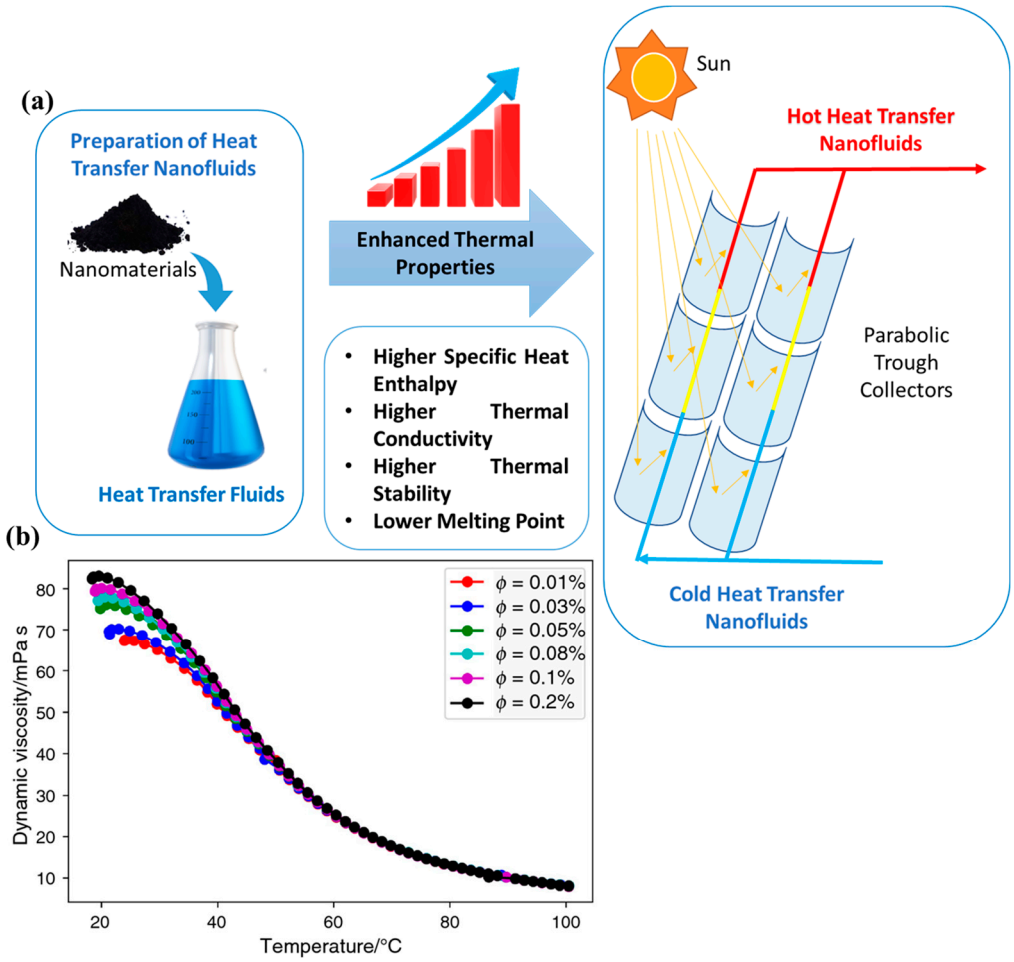

Figure 1. (**a**) Schematic illustration of the parabolic trough and heat transfer fluid collector; (**b**) experimental values of dynamic viscosity at various concentrations and temperatures [34].

2. Preparation of MXene

By etching specific atomic layers of the MAX layers, which are a sizable group of ternary carbides and nitrides with a double transition metal structure, MXene is created [32]. MXene is characterized by its general formula, $M_{n+1}X_nT_x$, and is synthesized from the precursor MAX phase, which has a general formula of ($M_{n+1}A_nT_x$). The variable "M" represents an early transition metal; "A" represents an element from groups 12 to 16 of the periodic table; "X" denotes carbon or nitrogen; "T" represents the surface termination or functional groups, such as fluorine (–F), oxygen (–O), or chlorine (–Cl); "x" indicates the number of surface functionalities; and n = 1, 2, etc. [36,37]. In the MAX phase, a layer is intercalated between an octahedral lattice composed of a strongly bonded M–X bond and a comparatively weaker M–A bond [37]. The first multilayered MXene was discovered in 2011 by etching a layer of the MAX phase [32]. The variety of MAX phases exceeds 70. In these, titanium-based MXenes have been thoroughly explored by several researchers [38]. In addition to carbides, other MXene structures containing nitrides and carbonitrides are being investigated for a variety of uses [39,40]. Figure 2 illustrates the graphical diagram of a different synthesizing process of MXene discussed in this article.

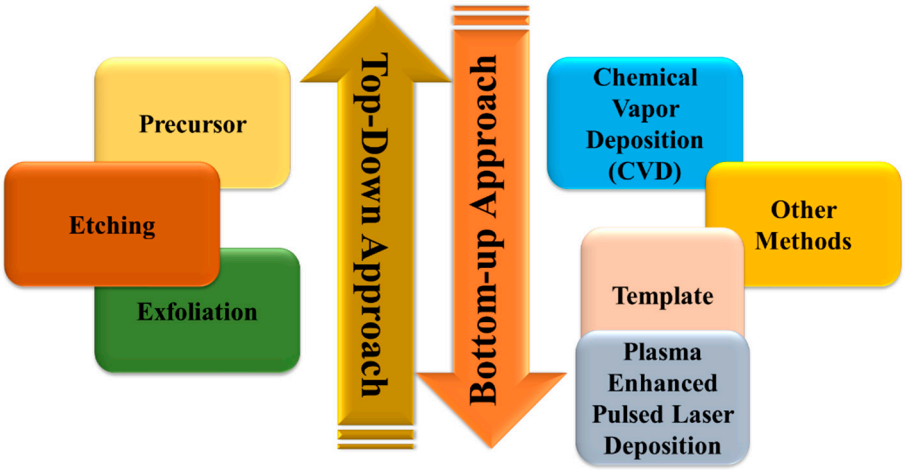

Figure 2. Fabrication methods of MXene by utilizing top-down and bottom-up approaches.

2.1. Top-Down Synthesis Approach

The top-down strategy, which includes several procedures like precursor, etching, and exfoliation, is mostly used to manufacture 2D MXene. In these procedures, the MAX phase is transformed into 2D MXene.

2.1.1. Precursor

More than 130 family groups with octahedra with A layer interlayers are found in the MAX phases [41]. The number of M layers between the A layers is as follows: 211, 312, or 413 are the main distinctions between these varieties [42]. The discovery of over 30 MXene materials has been made to date, all of which are synthesized through etching aluminum (Al) layers from Al-containing MAX phases. The preservation of the parent phases is crucial for maintaining the ordered structure of MXene materials. It is noteworthy that more than 50 MAX phases were first identified in the 1960s [43]. Additionally, two chemically ordered MAX phases were synthesized in 2014 and 2017: the o-MAX phases (312 or 413), which exhibit out-of-plane ordering, and the i-MAX phase 211, which demonstrates in-plane ordering. In contrast, the out-of-plane ordered MXene consists of a single or double layer of the M element sandwiched between layers of another M element [44]. The two M elements are plane ordered while in the i-MAX phase [45], and more recently, the i-MAX phase based on molybdenum has also been found, respectively [46].

2.1.2. Etching Strategy

The transformation of MAX to MXene involves altering the etched layers through the interaction with hydroxyl, oxygen, or fluorine. The stability of the resulting materials is maintained by van der Waals forces. Selective etching is the preferred method of MXene production, as the metallic M–A bond cannot be fabricated through mechanical means. Typically, 2D MXene is created using acidic aqueous fluoride solutions that selectively etch the A-element layer from MAX phases. The most widely utilized etching agent is HF, and the concentration of HF can be adjusted to produce MXene via HF acid etching in the temperature range of room temperature to 55 °C [47]. Furthermore, strong etching was necessary to accommodate the increase in "M's" atomic number. The metallic M–Al bond required a vigorous etching because of the high M valence electrons. Because HF has hazardous effects, it can be substituted for a strong acid and fluoride salt mixture while producing MXene [48]. One of the techniques is to use hydrofluoric acid (HF) or to produce HF locally by reacting HCl or fluoride acid, as LiF and HF acid combine to create HF in situ, resulting in the A layer being etched [37,49]. This method was first introduced by Ghidiu et al. [50] utilizing LiF and HCl on MXene ($Ti_3C_2T_x$), respectively.

Only Al was considered to have been etched from the MAX phase during the deterioration. Alhabeb et al. [51] proposed the utilization of in situ HF etching for preparation

purposes. They evaluated the effectiveness of 5%, 10%, and 30% weight concentrations of HF, with varying etching times of 5, 18, and 24 h, respectively. The results obtained were consistent across all conditions. Furthermore, an in-situ approach utilizing HCl and LiF as etchants was implemented, with etching exceeding 24 h. Most studies focused on this, making it not the only first MAX phase (Ti_3AlC_2) to be engraved. The first method of preparation involved soaking powder of (Ti_3AlC_2) in 50 wt% of HF [25]. As the conventional HF process requires about 10 h for preparation, Hu et al. [52] demonstrated the rapid production of 2D MXene through etching in a 40% HF solution for 0.5 h at a temperature of 50 °C with constant magnetic stirring. The produced MXene displayed stability up to 300 °C in air oxidation and up to 800 °C under vacuum.

2.1.3. Exfoliation Route

The primary method for producing high yields of colloids is liquid exfoliation through molecule intercalation is explained. The direct sonication approach can eliminate etching byproducts when multilayers are produced using an etchant other than HCl/LiF. It is crucial to introduce the right molecules to exfoliate multilayers into a single nanosheet since multilayers comprise cations and organic compounds. MXene may be exfoliated using the sonication or shaking method [53,54]. Exfoliation is achieved using the polar chemical compound DMSO [55]. The intercalation of DMSO leads to an increase in the interlayer d-spacing from 9.8 to 17.6 and can reach up to 22.4 when co-intercalated with water. This can be observed through the shift in the position of the (0002) peaks in the X-ray diffraction (XRD) pattern, which corresponds to the interlayer d-spacing [55]. Another method of exfoliating 2D materials involves the use of tetrabutylammonium hydroxide (TBAOH) [56], which relies on the intercalation of TBA^+ ions within the interlayer space. This approach has been widely utilized for exfoliating MXene materials.

2.2. Bottom-Up Processing Techniques

The bottom-up preparation process encompasses a range of techniques, including the template method, plasma-enhanced pulsed laser deposition (PEPLD), and chemical vapor deposition (CVD). Additionally, recent advancements in technology have also been incorporated into this process. The resulting high crystalline structure of the materials produced allows for specific comparisons to be made among these procedures.

2.2.1. Chemical Vapor Deposition (CVD) Route

The first thin film on MAX phases created using this method was on Ti_3SiC_2, which was the research of Nickl and co-workers [57]. Ti_3SiC_2 was formed using this method at high temperatures between 1000 and 1300 °C [47]. Additionally, Ti_3SiC_2 can be made by simultaneously depositing all components and interacting with the gas and solid phases during CVD [58]. Phase purity is also a concern at this temperature, which is usually higher. During the chemical vapor deposition (CVD) process, the species on the surface are taken up, leading to a decrease in surface diffusion. This method was demonstrated by Xu et al. [59] in the fabrication of films using a copper/transition metal bilayer metal foil. The stack was subjected to a temperature of 1085 °C in a hydrogen atmosphere for the growth of molybdenum carbide crystals, with a methane flow rate as the source gas. During the crystallization process, the top liquid layer of copper was extremely important. Additionally, the copper worked as a catalyst for synthesizing carbon from methane and as a conduit for the migration than melodeum atoms into liquid copper, resulting in the formation of ultrathin layers. However, rather of being made up of a single MXene sheet, the thinnest MO_2C layer was actually made up of six MO_2C layers, respectively.

Similarly, by combining rGO with MXene nanosheets, Yang et al. [60] created an ultrafine platinum NP-decorated 3D hybrid nanocomposite. The resulting nanocomposite demonstrated strong catalytic activity and long-term stability. Additionally, it was discovered that nanocomposite exhibited remarkable electro-catalytical characteristics for methanol oxidation. Additionally, Yang et al. [61] also formed quasi-1D Pt nano-worms

grown on MXene nanosheets functionalized with polydiallyldimethylammonium chloride (PDDA). The resulting nanocomposite demonstrated significant anti-poisoning properties, better stability and durability, and good electrocatalytic activity. By using ammonia as a nitrogen source, Wang et al. [62] were employed to create titanium carbides and titanium nitride Ta compounds. The copper foil was held in a solid state, and boron, rather than ammonia, was used to make ultrathin titanium bromide. Along this line, it was possible to adjust the size of 2D nanocrystals below the melting point of copper.

Furthermore, due to the thin layers that are formed rather than a single layer, this process is not used to prepare MXene. As a result, the top-down method is employed to manufacture MXene because the chemical vapor deposition method is unsuitable. Additionally, this approach has a high cost and produces little. Therefore, MXene preparation still needs optimization.

2.2.2. Other Fabrication Routes

The utilization of the template method in the production of 2D materials is implemented to achieve high yields, as the CVD results in low yields. This method employs 2D nanosheets composed of transition metal oxides, which are subjected to carbonization or converted into nitrides [63,64]. The type of transition metal oxide to be employed determines the structure of transition metal carbides or nitrides. Using this approach, Joshi et al. [65] created 2D hexagonal MoN nanosheets by heating ammonia to 800 °C to change 2D (MoO_3) nanosheets into MoN nanosheets. The formation of 2D MoN nanosheets resulted in a layered-like structure.

Furthermore, Zhang et al. [66,67] proposed a plasma-enhanced pulsed laser deposition technique to fabricate ultrathin Mo_2C films. This approach integrates CVD and pulsed laser deposition (PLD) methods. The films were produced by heating a sapphire substrate to 700 °C using methane as the carbon source. Despite this approach, the films produced were found to have poor crystalline quality and significant stacking defects.

3. Global Recent Progress on Phase Change Materials (PCM)

The main barrier to implementing solar energy is its irregular supply. In solar energy systems, there is constant impartiality between the supply and demand of energy that can be mitigated to some extent by using effective energy storage materials like PCMs. The world energy supply–demand gap has encouraged research on thermal energy storage, where PCMs emerged as the utmost capable substitute.

3.1. Phase Change Material and Its Classification

Phase change materials (PCM) are widely used as a thermal energy storage (TES) medium. During the phase change process, these materials can accumulate and release a significant amount of energy [17]. Daylight-based solar radiation has shown tremendous potential in the application of PCMs. The utilization of PCMs in solar energy systems is particularly prevalent in cogeneration systems, where it can significantly reduce power consumption during peak hours of usage. The application of PCMs also reduces the need for additional equipment, resulting in a decrease in power requirements, which is a major advantage of this technology [68]. Sensible heat storage refers to the absorption or transmission of heat from one substance to another without a change in its current phase. On the other hand, latent heat storage occurs during a phase transition, where a substance absorbs heat from the environment as it undergoes an endothermic process. PCMs are widely recognized as efficient latent heat storage materials. However, it is important to note that, before reaching their melting point, PCMs absorb heat sensibly. During the melting process, PCMs continue to absorb heat until they become fully molten. The melting period of PCMs is influenced by several factors, including their volume, thermal conductivity, and any components that aid in the transmission of heat. Once the PCM has fully melted, it starts to absorb heat sensibly once again, as shown in Figure 3.

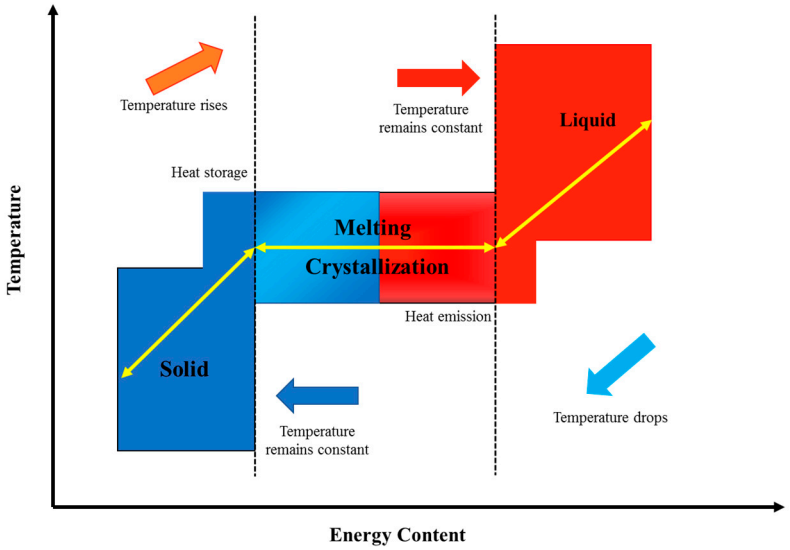

Figure 3. Phase changing phenomenon.

Over a certain temperature range, PCMs have the ability to absorb and store energy. The kind of material, thermal characteristics, and chemical structure all substantially impact the phase transition temperatures of the PCMs [69,70]. PCM is a thermally active substance that can absorb and release a significant amount of heat energy through melting and solidifying at a specific temperature. There are three main categories of PCMs: organic, inorganic, and eutectic. Organic PCMs consists of paraffin or non-paraffin carbon-containing compounds, while inorganic PCMs comprise salt hydrates and metallics. Eutectics are composed of a mixture of two or more compounds. A classification of PCMs is presented in Figure 4 [17].

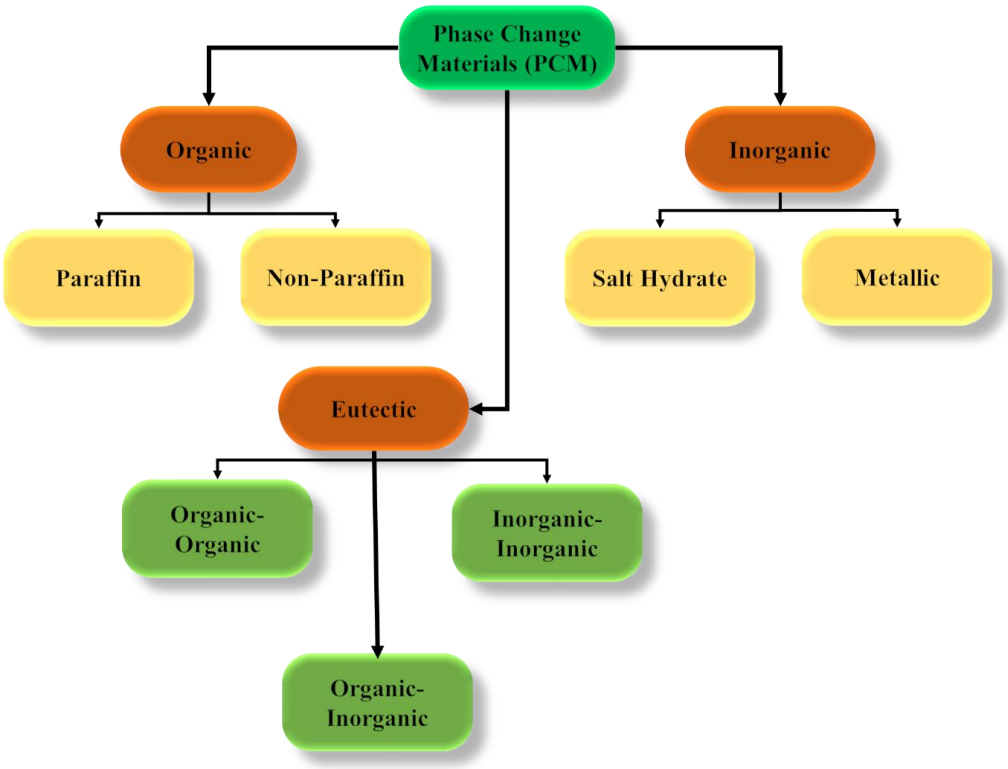

Figure 4. Classification of PCMs.

3.2. PCM Selection

The efficiency of solar energy systems is largely dependent on the efficacy of thermal energy storage technology due to the unpredictable and sporadic nature of solar exposure. Traditional methods of accumulating solar thermal energy, such as sensible heating through solar thermal collectors or photovoltaic thermal collectors, are limited by the large volume of water required to store a significant amount of heat. The integration of PCM with sensible and latent heat storage provides a solution to this issue by offering increased heat accumulation per unit volume. PCMs absorb heat as they transition from a solid to a liquid state during periods of high solar exposure and release it during periods of low solar exposure. The presence of PCMs in water can result in increased heat absorption and slower heat loss, leading to improved efficiency in solar thermal systems. Using latent heat storage technology in PCMs provides improved temperature stability of stored hot water and, therefore, increases the overall capacity for heat storage in solar thermal systems.

Choosing a material with the appropriate thermal properties in one might be challenging despite the advantages of utilizing PCM for thermal regulation in PV or other solar systems. It is difficult to choose a PCM methodically because a given chemical may have some positive traits while also having some detrimental traits in relation to thermal management. The PCMs used the most in solar energy storage systems are those made by Rubitherm Technologies GmbH, Berlin, Germany, and they are designated as RT20, RT21, RT25, RT27, RT31, RT35, RT42, RT60, RT10HC, RT18HC, RT25HC, and RT35HC. Properties of the most used paraffin wax PCMs for solar energy applications are given in Table 1. Additionally, selecting the best PCM modifies the performance of PV systems, and the criteria of the PMCs are summarized in Figure 5 [71].

Table 1. Properties of the commonly used paraffin wax-based PCMs for solar energy applications.

Base PCM	Melting Temperature (°C)	Latent Heat of Fusion (kJ/kg)	Specific Heat Capacity (kJ/kgK)	Thermal Conductivity (W/mK)	Reference
RT20	21.23–25.73	140.3	1.8–2.4	0.2	[72]
RT21	21	134	n.a.	0.2	[73]
RT25	26.6	232	1.8–2.4	0.19	[74]
RT27	26–28	184	1.8–2.4	0.2	[75–77]
RT31	29	169	1.82	0.2	[73]
RT35	35	157	1.78–2.37	0.2	[76]
RT42	38–43	174	2.0	0.2	[78]
RT44	41–45	255	2.0	0.2	[79]
RT60	60	144	n.a.	0.2	[73]
RT10HC	9	126	2	0.2	[80]
RT18HC	17	222	2	0.2	[80]
RT25HC	22	177	2	0.2	[80]
RT35HC	34	197	2	0.2	[80]

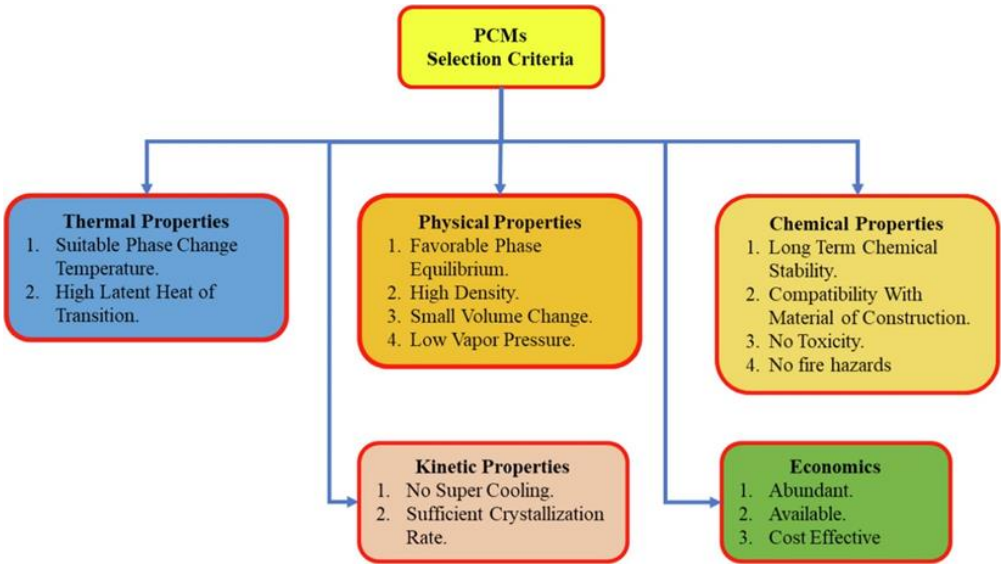

Figure 5. Various criteria for the selection of PCM [71].

4. Phase Change Materials under Thermal Regulation of Solar Thermal Energy Storage Applications

4.1. Selection of Nanoparticles and MXene

The improvement in the thermal conductivity of PCMs is crucial for their use in thermal applications. The thermal conductivity of base PCMs can be enhanced using various methods, such as the addition of nanoparticles (nanopowders, nanowires, nanotubes), impregnation, and modification of the blades. This is significant because an improvement in thermal conductivity will improve the melting rate of the PCM [81,82]. It has been observed that the addition of nanoparticles increases the dynamic density of the PCM, which in turn affects convective heat transfer [83]. The choice of nanoparticles depends on several factors, including thermal conductivity, particle size, price, volume fraction, and kind of base fluid, among others [84]. The reduction of particle size to the nanoscale increases surface area relative to volume, thereby enhancing the dispersion of the base PCM. This makes particle size a critical factor in determining the thermal conductivity of the system. Experimental data indicate a positive correlation between particle size reduction and thermal conductivity improvement. Furthermore, high-concentration nanoparticle mixtures exhibit longer melting times compared to pure PCMs and low-concentration nanoparticle mixtures. This can be attributed to the increase in dynamic viscosity as a result of the rise in nanoparticle concentration. The elevated dynamic viscosity results in reduced buoyancy-driven natural convection, which is the predominant mechanism of heat transfer during the melting process. Thus, the overall rate of melting is hindered, emphasizing the importance of particle size in influencing the thermal performance of nanoparticle-based PCMs [85,86]. Therefore, MXene materials possess a range of properties, including structural, optical, and electrical properties, and in some cases, high thermal energy storage capabilities, as depicted in Figure 6 [87,88]. These properties enable MXenes to be utilized in multiple applications, with a particular emphasis on thermal energy storage. Additionally, the presence of hydrophilic functional groups grants MXenes the capability to store solar thermal energy [89].

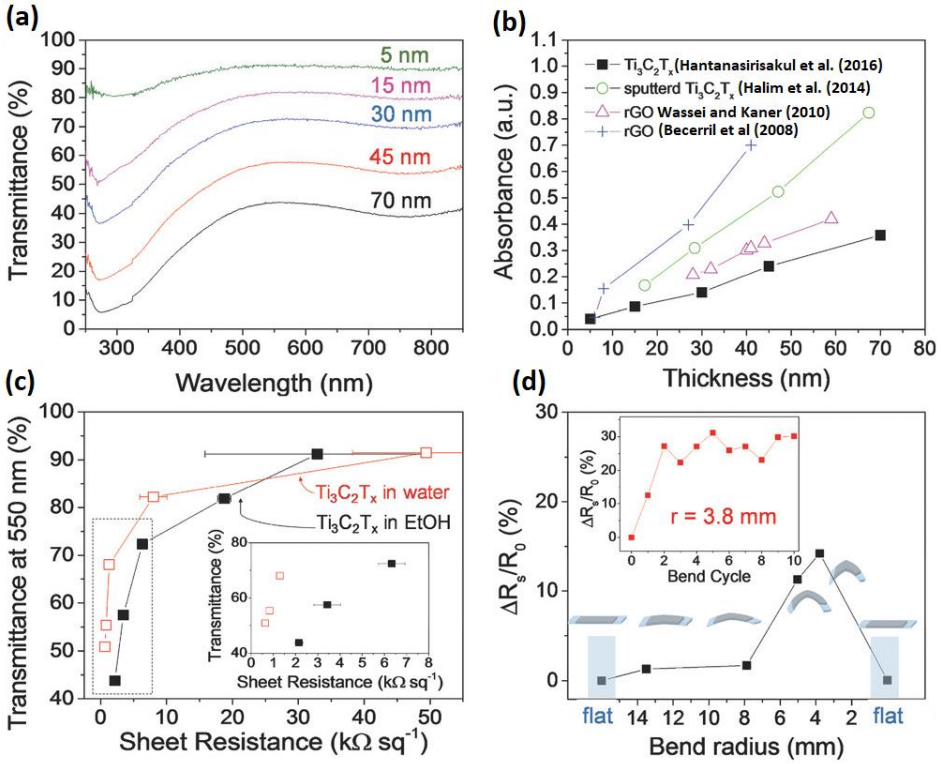

Figure 6. (**a**) UV–vis spectra of $Ti_3C_2T_x$ films with different thicknesses. (**b**) Effect of thickness on absorbance of $Ti_3C_2T_x$ [90] films compared with $Ti_3C_2T_x$ [91], rGO [92], rGO [93]. (**c**) Sheet resistance versus transmittance at 550 nm of $Ti_3C_2T_x$ sprayed from ethanol and water solutions. The inset shows the low sheet resistance region. (**d**) Bending test of a film on a flexible polyester substrate [90].

4.2. MXene-Based Phase Change Materials

Wang et al., synthesized a vertically oriented network composite PCM by utilizing reduced graphene oxide/MXene hybrid aerogels (rGO/MXene) as the supporting matrix and encapsulating stearic acid as the PCM. The thermal conductivity of the composite was found to be 317.24% higher than stearic acid [94]. Liu et el. [95] fabricated a high-performance phase change composite material by confining MXene within a shape-stabilized phase PCM. This combination resulted in a simultaneous enhancement of both electromagnetic interference shielding (EMI) and thermal conductivity. The EMI of the MXene/PCM composite was found to be 64.7 dB in the X-band, with an improved thermal conductivity of 0.74 W/mK. The DSC curves of PEG, PCM, and MXene/PCM are illustrated in Figure 7, and the thermal conductivities of PCM and MXene/PCM have been investigated, as shown in Figure 8 [95]. Du et al. [96] synthesized composite phase change materials (PCMs) by incorporating melamine foam (MF) and MXene through a polydopamine (PDA) process, which was used to enclose polyethylene glycol (PEG) to produce a composite PCM (CPCM). The study results indicated that the proposed PEG/MPMF CPCM (PEG@MPMF) exhibits satisfactory thermal energy storage characteristics, with a melting enthalpy of 186.2 J/g, which constitutes 99.5% of the pure PEG value. Wang et al. [97] reported a facile strategy for fabricating MXene-decorated non-PCM emulsions (NPCMEs) that possess excellent stability, minimal supercooling, and high thermal conductivity, achieved through the self-assembling of MXene nanosheets at the PCM/water interface. The findings revealed that the MXene concentration plays a significant role in determining the average droplet diameters, stability, and thermophysical properties of the NPCMEs. The thermal conductivity of the 10 wt% n-tetradecane/water NPCME MXene was 0.693 W m^{-1} K^{-1}, resulting in an improvement of 15.5% compared to that of water. Sheng et al. developed a novel bio-based pomelo peel foam (PPF)/polyethylene glycol (PEG) composite PCM that was designed and prepared via the simple impregnation process. The resulting PCM was

modified with a low concentration of MXene nanosheets to enhance its optical-to-thermal energy conversion efficiency, thermal energy storage capacity, and thermal conductivity. The thermal conductivity of obtained PPF@MXene/PEG FCPCMs was also improved (from 0.25 to 0.42 W/mK) [98]. Khan et al. [99] reported the titania and MXene-based PCM for the thermal storage of energy. The direct synthesis method was utilized to fabricate and incorporate the nanoparticles (NPs) in paraffin wax (PW82) for the production of nano-enhanced phase change material (NEPCM). An investigation was carried out to evaluate the hybrid nano-enhanced PCM in PW82 using wt% ratios of 0.1, 0.2, and 0.3 of TiO_2 and MXene. The specific heat capacity of the PCM was improved through the doping of titania and MXene, leading to an increase in specific heat of 41.3% with a 0.3 wt% doping of TiO_2-Ti_3C_2. A maximum increase in thermal conductivity of 15.6% was discovered with a doping of 0.3 wt% TiO_2-Ti_3C_2. The dissociation temperature of the produced NEPCM rose by approximately 6% with a 0.3 wt% weight fraction. The results of this study demonstrate the significant potential to improve the heat storage capacity of organic paraffin by doping TiO_2 and Ti_3C_2 with PW82 to produce a novel class of NEPCMs.

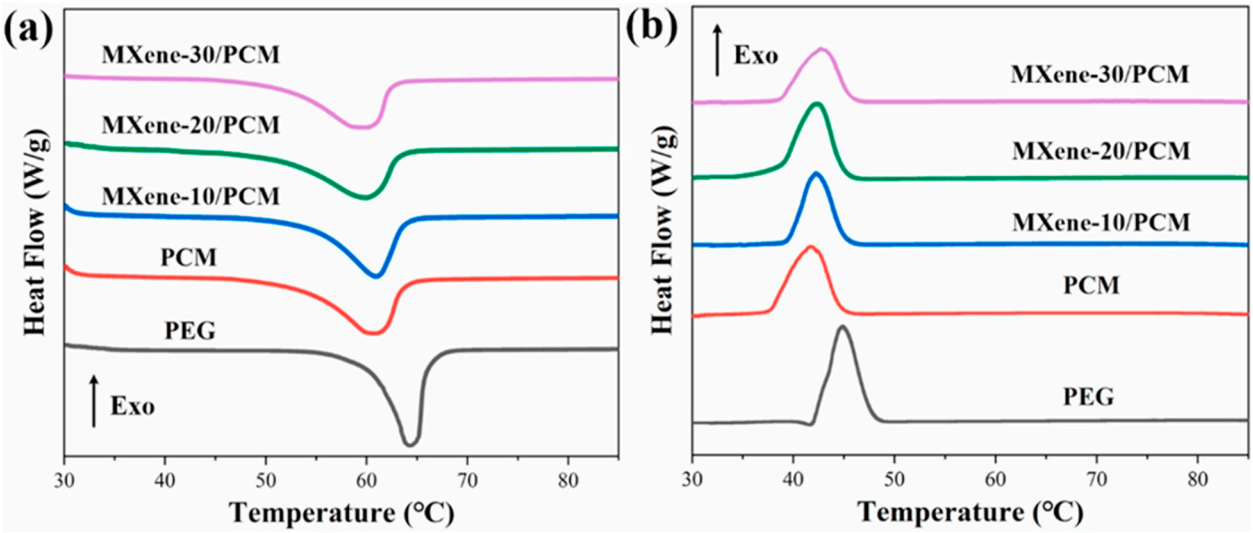

Figure 7. DSC curves of PEG, PCM, and MXene/PCM: (**a**) heating process and (**b**) freezing process [95].

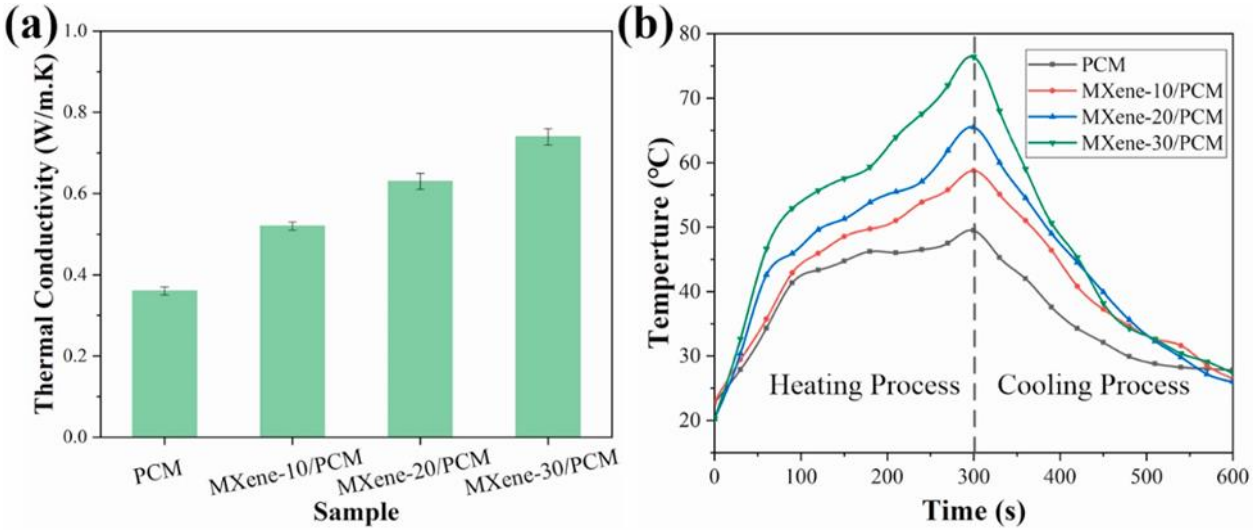

Figure 8. (**a**) Thermal conductivity of PCM and MXene/PCM; (**b**) temperature evolution curves of PCM and MXene/PCM during the heating and cooling process [95].

In a study by Luo et al. [100], a flame-retardant PCM was successfully synthesized through the chemical modification of stearyl alcohol (SAL) with a phosphorus-containing molecule. The resulting form-stable phase change composite was manufactured through a vacuum impregnation procedure utilizing an MXene with a porous structure as the supporting backbone for the PCM. The MXene-based PCMs demonstrated a significant thermal conductivity of 0.486 W m^{-1} K^{-1}, attributed to the high aspect ratio and strong capillary force of the MXene aerogel as well as the interfacial interaction between the PCM molecule and the MXene. Cheng et al. employed melamine foam (MF) as a template to fabricate a continuous thermal/conductive network through dip coating with magnetized nickel (Ni)/MXene (NiM). Subsequently, polyethylene glycol (PEG) was incorporated into the porous NiM/MF hybrid sponge via a vacuum impregnation technique. The resulting NiM/PCM exhibited desirable thermal conductivity (0.39 W/mK) and electrical conductivity (76.3 S/m) due to the synergistic effect of magnetic Ni chains and highly conductive MXene, as well as excellent EMI shielding effectiveness (34.6 dB) [101]. Shao et al. [102] developed novel PCM composites by incorporating MXene-coated melamine foam (MF@MXene) into poly(ethylene glycol) (PEG). The resulting PCM composites displayed excellent encapsulation properties, superior solar-to-thermal conversion efficiency, and shape memory functionality. Gao et al. [103] reported the olefin block copolymer acted as the polymer substrate, and paraffin was utilized as the PCM merged with MXene for flame retarding and self-healing for thermal applications. They discovered that the MXene-based layered porous structure and OBC-dependent polymer network achieved double-coupling encapsulation of PA, resulting in a PA/OBC/MXene CPCM with superior thermal stability and high relative enthalpy efficiency (97%).

In a study by Krishna et al. [104], a novel nanocomposite consisting of palmitic acid and Ti_3C_2 MXene was synthesized through a two-step process. The results indicated an increase in enthalpy by 4.34% and thermal conductivity by 14.45%, suggesting that the nanocomposite has the potential for use in TES applications. Wang et al. [105] prepared Ti_3C_2/pectin aerogels using a solution blending method to self-assemble pectin and MXene nanosheets (Ti_3C_2). The aerogels were immersed in molten dodecylamine (DDA) as a phase change material. The findings indicated that the phase change temperature of the PCM composites, containing 3 wt% Ti_3C_2, was 25.47 °C, and the thermal conductivity was 0.1817 W/(mK). Du et al. [106] conducted a study to synthesize novel phase change material (PCM) composites with improved thermal conversion efficiency, form stability, and thermal conductivity. The study utilized dopamine-decorated MXene ($Ti_3C_2T_x$@PDA) and polyethylene glycol (PEG)-based polyurethane as the PCM. The resulting PCM composites exhibited excellent form stability, remarkable thermal reversibility, good thermal stability, and improved thermal conductivity. Furthermore, Ji et al. fabricated a composite film by impregnating an organic PCM into a surface-modified MXene/bacterial-cellulose aerogel. The resulting aerogel-based PCM film exhibited increased loading capacity of the organic PCM, increased phase change latent heat, and improved mechanical properties [107]. Fan et al. [64] synthesized a novel composite phase change material (PCM) comprised of polyethylene glycol (PEG) and $Ti_3C_2T_x$ nanosheets, which demonstrated superior photothermal storage capabilities due to its stacked nanosheet structure and PEG filling. This composite showed a significant absorption of electromagnetic waves in the UV-Vis-NIR region. Mo et al. [108] further developed this concept by creating a PEG 2000 composite supported by a $Ti_3C_2T_x$@polyvinyl alcohol (PVA) foam structure. The thermal conductivity of the composite, containing 7.68 weight% skeletons, was found to be notably high, with a value of 0.428 W/mK, which was 4.2 times higher than that of pure PEG 2000 (0.101 W/mK).

5. Solar Thermal Energy Application

Due to their remarkable qualities and viability, MXene-based materials are used in a wide variety of applications. Among these are applications in thermal, electrical, optics,

electronics, electrochemistry, catalysis, sensors, biomedicine, and environmental technology. In this section, only applications related to heat will be covered in depth.

5.1. MXene Architect PCM for Solar Energy (SE) Applications

MXene-based materials in solar energy applications have become widespread due to their ability to maximize the utilization of solar energy and improve energy conversion efficiency. Jiang et al. [109] conducted a study to evaluate the properties of this 2D material, which consists of MXene nanosheets (NPs). Their findings revealed that these NPs exhibit exceptional optical characteristics across the wavelength range of 800–1800 nm. The high absorption coefficient and nonlinear refractive index were noted as key factors contributing to the broad wavelength range for light signals.

Similarly, to improve PCM's thermal properties, Aslfattahi et al. [35] incorporated MXene-based NPs as an additive in the organic phase change material. The study involved adding three different concentrations (0.1–0.3 wt%) of MXene NPs to the paraffin wax (PW70). Several parameters were analyzed to evaluate thermal and optical properties, including thermal conductivity, specific heat capacity, and absorbance capacity. The addition of 0.3 wt% MXene NPs in the PCM resulted in a substantial increase in absorbance capacity in the UV-Visible spectrum, demonstrating an improvement of 39% compared to the pure PCM. The integration of 0.3 wt% MXene NPs into the PCM also showed significant enhancement in thermal conductivity and specific heat capacity, with an increase of 16% and 43%, respectively. Fan et al. [64] reported PEG/$Ti_3C_2T_x$ MXene composite PCM to enhance grid storage for solar heating applications. Ultrathin MXene nanosheets that served as a supporting structure for the PEG encapsulation were used to create the composite. Regarding solar radiation absorption in the near visible and near-infrared area, the PEG and MXene composite showed remarkable performance. Moreover, the photothermal conversion efficiency reached 94.5% under actual solar radiations and demonstrated form stability both before and after the phase transformation, as seen in Figure 9a,b.

Lin et al. [110] proposed using a 2D transition-metal carbides/carbonitrides MXene aerogel-based PEG phase change material for solar energy applications following the same concept. MXene nanosheets were combined with PEG and then frozen to create the composite. The produced MXene/PEG composite had a high extinction coefficient in the UV-Vis-NIR band at 380 nm and was lightweight. The near-infrared region of Figure 9c shows the absorption band features of the MXene colloid. Improvements were made to PEG's thermal stability, and the thermal decomposition temperature was raised to 40 °C. The MXene/PEG composite had a photothermal storage efficiency of up to 92%. Moreover, when the sun is not shining, MXene@PEG aerogels can gradually release the thermal energy they have stored for a specified purpose to the environment. Similarly, the MXene@PEG aerogels can begin a new energy conversion, storage, and release cycle when the solar energy reappears, as portrayed in Figure 9d. Furthermore, Figure 9e shows the MXene@PEG aerogels' light-to-heat energy conversion measurements. In order to regulate the intensity of light in a solar simulator, a digitizer and a blocker are utilized in the light beam, resulting in light intensity of 100 mW/cm^2. Simultaneously, PEG4000 and PEG10000 are subjected to heating from room temperature to 43.5 °C and 35.1 °C, respectively, which are within their respective melting points of 60.2 °C and 63.4 °C. The primary contributors to this phenomenon are the intense reflection of light by the white coverings and the inadequate light conversion. Despite the significant rise in temperature of the MXene@PEG aerogels (PEG4000 and PED10000) with an increase in irradiation duration, the average maximum temperature remains above the melting thresholds. This is due to the strong light absorption by the MXene nanosheets in the aerogels. The temperature evolution graphs indicate a turning point during the light-on process when the MXene@PEG aerogels begin to fuse, signifying the simultaneous storage and generation of heat by PEG and the MXene nanosheets. Upon switching off the simulated sunlight, the temperatures of the MXene@PEG aerogels rapidly decrease due to heat exchange with the environment and the release of latent heat during solidification. The photothermal storage

efficiencies of MXene@PEG aerogels (PEG4000) range from 92.5% to 55.6%, with an increase in MXene concentration from 5% to 30%. Similarly, the photothermal storage efficiencies of MXene@PEG aerogels (PEG10000) range from 85.5% to 51.6%, with the same increase in MXene concentration. The photothermal storage efficiency is positively correlated with the MXene content, as a higher concentration results in improved optical absorption in the visible and infrared regions, as seen in Figure 9f,g.

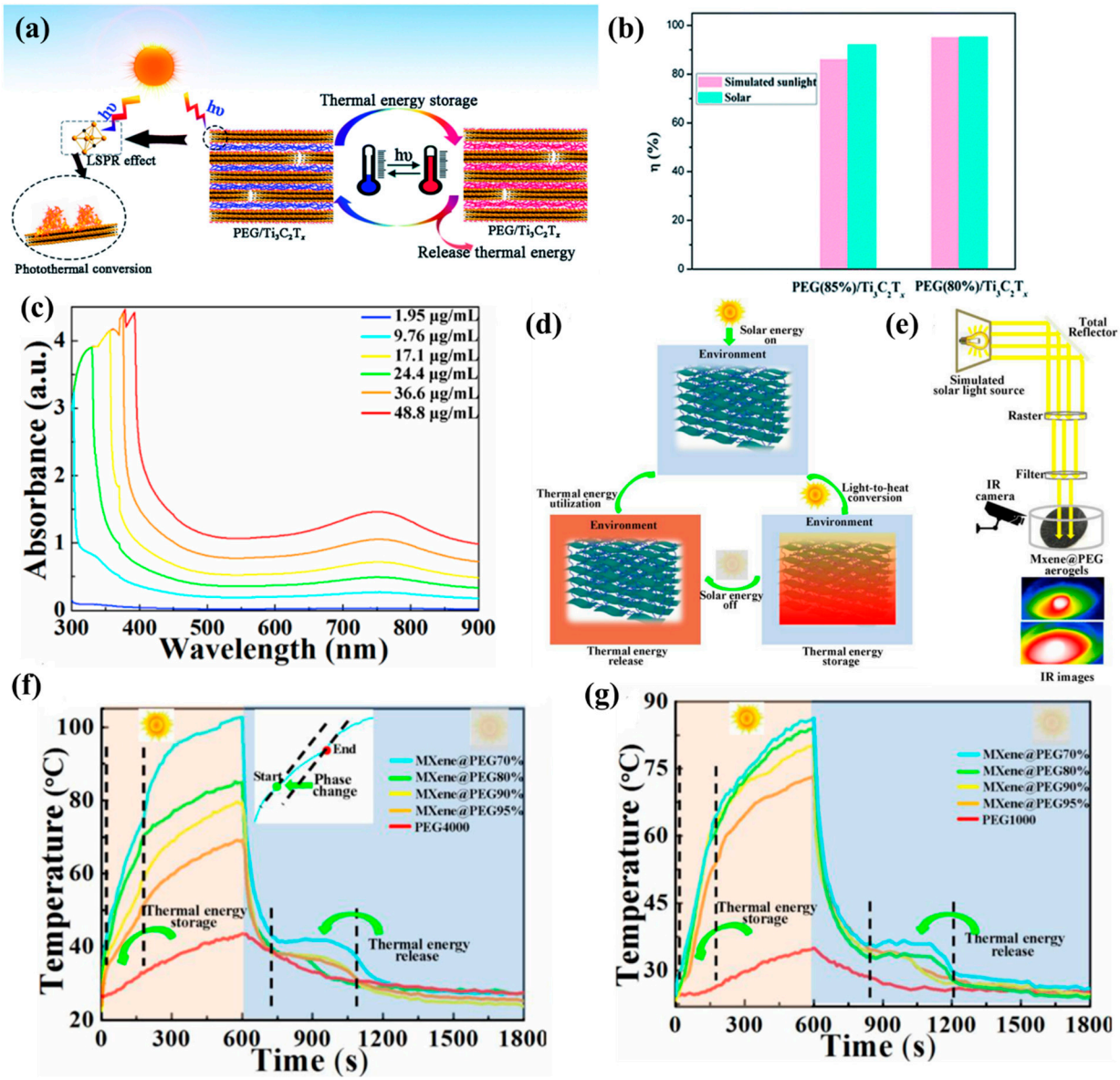

Figure 9. (**a**,**b**) Schematic diagram for the mechanism of photothermal energy conversion (PTE) and storage of the PEG- and MXene-based $Ti_3C_2T_x$ composites and the PTE efficiencies of the fabricated composites under the simulated and real sunlight irradiation [64]. (**c**) UV–Vis–NIR absorption spectra of MXene colloids with various concentrations at room temperature. (**d**–**g**) The photothermal effect drives SE conversion and storage: schematic diagram of the light-to-heat conversion and storage of prepared aerogels. Experimental arrangement for fabricated materials. Temperature calculation curves of bare PEG and MXene@PEG aerogels at (PEG4000 and PEG10000) respectively [110].

Lu et al. [111] reported the composite of PEG@MXene, where PEG was used as the PCM while MXene NSs served as the thermally conductive fillers in the vacuum impregnation procedure used to create the composite. PEG helps to increase the PEG's crystallization and serves as heterogeneous crystal nuclei, whereas, according to DSC and

XRD test, the results revealed that the relative thermal conductivity and EC of PEG@MXene were 2.052 W/mK and 10.41 S/m, respectively, and that the relative enthalpy efficiency was 80.3%. On the contrary, the melting and freezing latent heat values of PEG@MXene were 131.2 J/g and 129.5 J/g, respectively (Figure 10a,b).

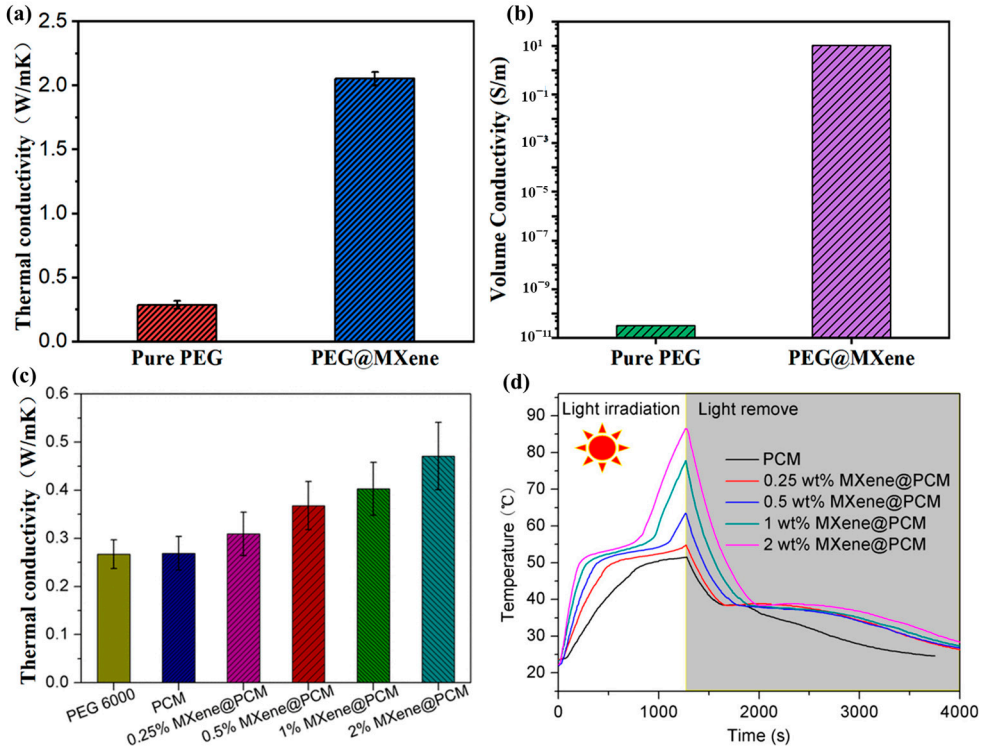

Figure 10. (**a**,**b**) Thermal and electrical conductivity of pristine PEG and fabricated PEG@MXene [111], (**c**) Thermal conductivities of PEG 6000, PCM, and MXene@PCMs, (**d**) Temperature evolution curves of the PCM and MXene@PCMs [106].

Besides, according to Wang et al. [112], the excellent photothermal conversion efficiency of MXene-based optimum modulators makes them suitable for solar energy applications. The optical modulation depth and spectrum range of the MXene-based 2D materials are 27 dB and 16.8 nm, respectively. The authors reported solar energy consumption applications would greatly benefit from photonics research based on 2D materials. Furthermore, in order to effectively transform solar energy into thermal energy, Du et al. [106] produced PEG-based polyurethane (PU) PCM coated with dopamine. The composite PCM produced excellent thermal conductivity, form stability, and thermal stability, as shown in Figure 10c. However, the resulting composite absorbed and stored thermal energy by transitioning from a solid–solid phase. The phase change enthalpy ranged from 121.9 to 128.2 J/g according to the results of the differential scanning calorimeter. On the contrary, Figure 10d demonstrates the temperature progression curves for PCM and MXene@PCM under a 250 mW/cm^2 radiation dose. Specifically, the temperatures of the MXene@PCMs increased significantly while $Ti_3C_2T_x$@PDA efficiently collected photons and transformed them into thermal energy. Platforms (between 50.5 and 56.5 °C) could be seen in the temperature evolution graphs when the composites were heated to the phase transition temperature, suggesting that the generated thermal energy was stored in PCMs as latent heat. The MXene@PCM temperatures dropped when the light irradiation was stopped, and cooling platforms occurred between 50.0 and 47.2 °C due to the latent heat being released. Temperatures of PCM, 0.25, 0.5, 1, and 2 wt% MXene@PCM under illumination for 1270 s were 51.5, 54.8, 63.5, 77.8, and 86.6 °C, respectively. Additionally, the efficiency of solar–thermal conversion and storage was determined, and the results showed that the PCM composites were 64.2%, 71.9%, 83.2%, and 90.1% for MXene@PCM weights of 0.25,

0.5, 1, and 2, respectively. Thus, it was shown that the addition of the MXene $Ti_3C_2T_x$@PDA greatly enhanced the solar–thermal conversion performance of the PCM composites.

5.2. Photothermal Conversion Applications

Photothermal conversion is the process of harvesting light and turning it into heat as a final form of energy [113]. Broadband absorption and high light-to-heat conversion efficiency are anticipated in photothermal materials [114,115]. Due to the high localized surface plasmon resonance (LSPR) effect, which often occurs in metal nanoparticles, the peculiar structure of MXene materials gives them excellent solar spectrum absorption [116]. Compared to other 2D nanomaterials, such as graphene oxide or graphene, which exhibit broad absorption in the ultraviolet to near-infrared region, MXene demonstrates a more focused absorption in the same spectral range [117]. On the other hand, it is well known that MXene materials have exceptional EMI shielding effectiveness [118] and that most unintellectual EMI waves are subsequently absorbed as heat inside MXene nanosheets. One significant photothermal conversion mechanism for MXene materials is the substantial absorption of electromagnetic waves, which span a wide range of the solar spectrum, as illustrated in Figure 11a. Despite the limited understanding of the photothermal process in MXenes, there has been a growing interest in their exceptional photothermal conversion capabilities. Utilizing a droplet-based system that incorporates light absorption and heat measurement, Wang et al. [119] conducted a precise assessment of the light-to-heat conversion efficiency of MXene. The study utilized a laser beam with a fixed power density and spot size, operating at 473 nm or 785 nm, which was directed towards an aqueous droplet solution containing MXene (Figure 11b).

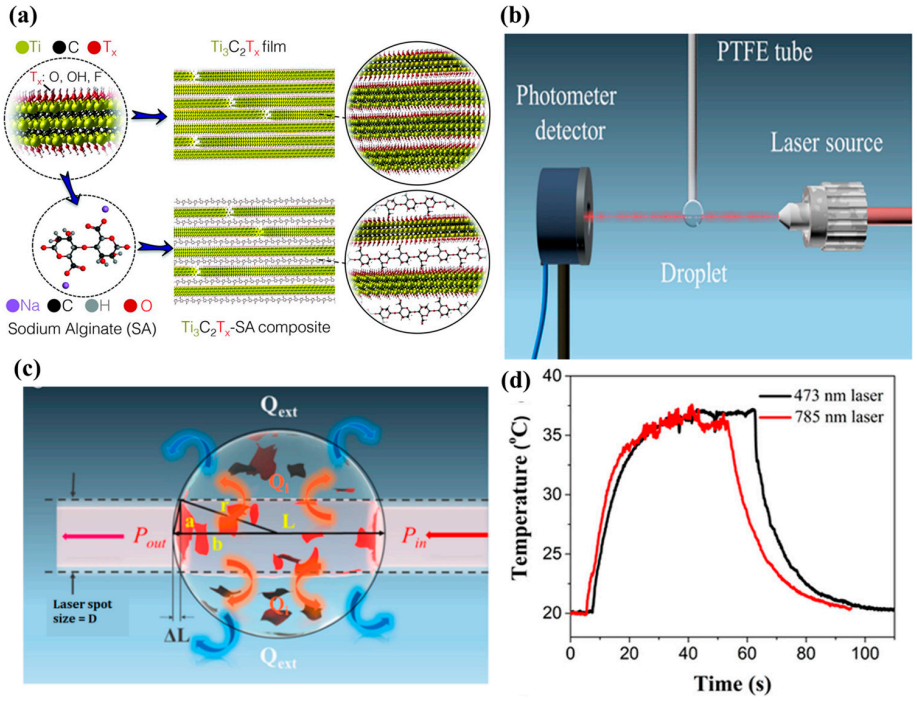

Figure 11. (**a**) Electromagnetic shielding interference mechanism of MXene [118]. (**b**) Experimental arrangement for droplet-related light-to-heat conversion [119]. (**c**) Schematic illustration of the droplet mechanism with laser irradiation [119]. (**d**) Time course of temperature profile of the droplet containing 0.1 mg/mL MXene in the light-to-heat conversion experiment under two separate laser irradiations [119].

Moreover, the incident laser beam energy within the droplet was assimilated by the MXene, resulting in a transformation into heat, causing a proportional increase in the droplet temperature. The data obtained indicated that MXene's light-to-heat conversion efficiency was close to 100%, regardless of the wavelength of the laser source. This high-

lights the exceptional photothermal conversion properties of the material, as depicted in Figure 11c,d.

5.3. Electrothermal Conversion Applications

MXene materials have demonstrated potential as Joule heating materials in various forms such as textiles, fibers, films, etc. This is due to their metal-like conductivity, with values reaching 106 S/m. For example, highly conductive and hydrophobic textiles have been fabricated by layering polymerized PPy-modified MXene NSs onto PET textiles, followed by a silicone coating. The PPy/MXene-patterned cloth had a good Joule heating capability and a high electrical conductivity of about 1000 S/m, which allowed it to quickly achieve a saturated temperature, as portrayed in Figure 12a,b [120]. The I-V curve showed the textile's low resistance, providing safe moderate-voltage heating with exceptional stability and recyclability. Additionally, the applied voltage may be adjusted to range from 40 °C under 2 V to 79 °C under 4 V, allowing for easy tuning of the saturation temperature. Similar to wearable photothermal heaters, textile-based Joule heaters require the ability to be knittable and shape-adapted for practical applications, for which direct modification of the fiber is a successful tactic. In order to create flexible, sewable MXene-decorated PET thread, Park et al. [121] electrostatically assembled negatively charged MXene flakes onto a positively treated PET fiber surface. These MXene/PET threads could be sewn and woven in varied shapes to accommodate diverse wearable heating circumstances.

It is interesting to note that MXene materials' higher photothermal conversion performance can combine with their Joule heating capacity to achieve all-weather heating. For instance, the utilization of 3D MXene aerogel, which has the capability to undergo simultaneous Joule heating and light heating, leads to the generation of steam under all weather conditions continuously. By regulating the applied voltage and solar irradiation energy, the temperature of the MXene aerogel can be set to the desired levels, resulting in the ability to generate steam even in low-light conditions. The combination of solar and Joule heating results in a significantly improved evaporation rate and energy conversion efficiency. This exceptional synergistic effect was mostly related to the sample's elevated surface temperature and the system's decreased relative humidity above the sample [122].

5.4. MXene Phase Change Materials in Electronic Applications

Due to higher cooling outcomes, MXene-based PCMs are frequently used in electronic cooling components. The polyvinyl chloride/MXene nanocomposite was created and described by Mazhar et al. [123] for use as thermal energy storage in electronic applications. After being prepared by HF etching, the delaminated MXene was combined with PVC at various concentrations using the solution casting procedure and sonication. The thermal conductivity was raised by 3.48 W/mK, thermal stability up to 683.6 °C was reached, and greater mechanical stability with tensile strength up to 174.08% was achieved. The enhancement of composite thermal conductivity is attributed to an increase in MXene loading. The results indicate a positive correlation between the thermal conductivity value and MXene content, where a higher loading of MXene results in a corresponding increase in thermal conductivity.

Moreover, for usage in electronics, Borysiuk and group [124] explored the thermal stability of titanium carbides, such as Ti_2C MXene, Ti_3C_2 MXene, and Ti_4C_3 MXene, respectively. To gauge the behavior of MXene, factors like the Lindemann Index, radial distribution function, and atomistic configuration were taken into account. The atomistic simulation models suggested the melting temperatures were 1050 K for Ti_2C, 1500 K for Ti_3C_2, and 1700 K for Ti_4C_3. The results indicated that, while MXene's melting temperature was lower than graphene, it can still be used in electronic components where heat dissipation is a major factor determining performance. Furthermore, a multilayered structure constructed from multilayered casting and based on PVA/MXene was presented by Jin et al. [125] for electronic purposes. The composite material, designed with a flame-retardant function, displayed elevated thermal conductivity and EC due to its minimal heat- and

electron-conducting network. The composite consisted of 19.5 wt% of MXene, which was 23 times greater in quantity compared to PVA. The composite displayed EC of 716 S/m and thermal conductivity of 4.57 W/mK. The material demonstrated high electromagnetic interference (EMI) shielding effects with a maximum measurement of 44.3 dB and the highest specific EMI shielding effect of 9343 dBcm^2/g. This performance is attributed to its use in advanced electrical applications.

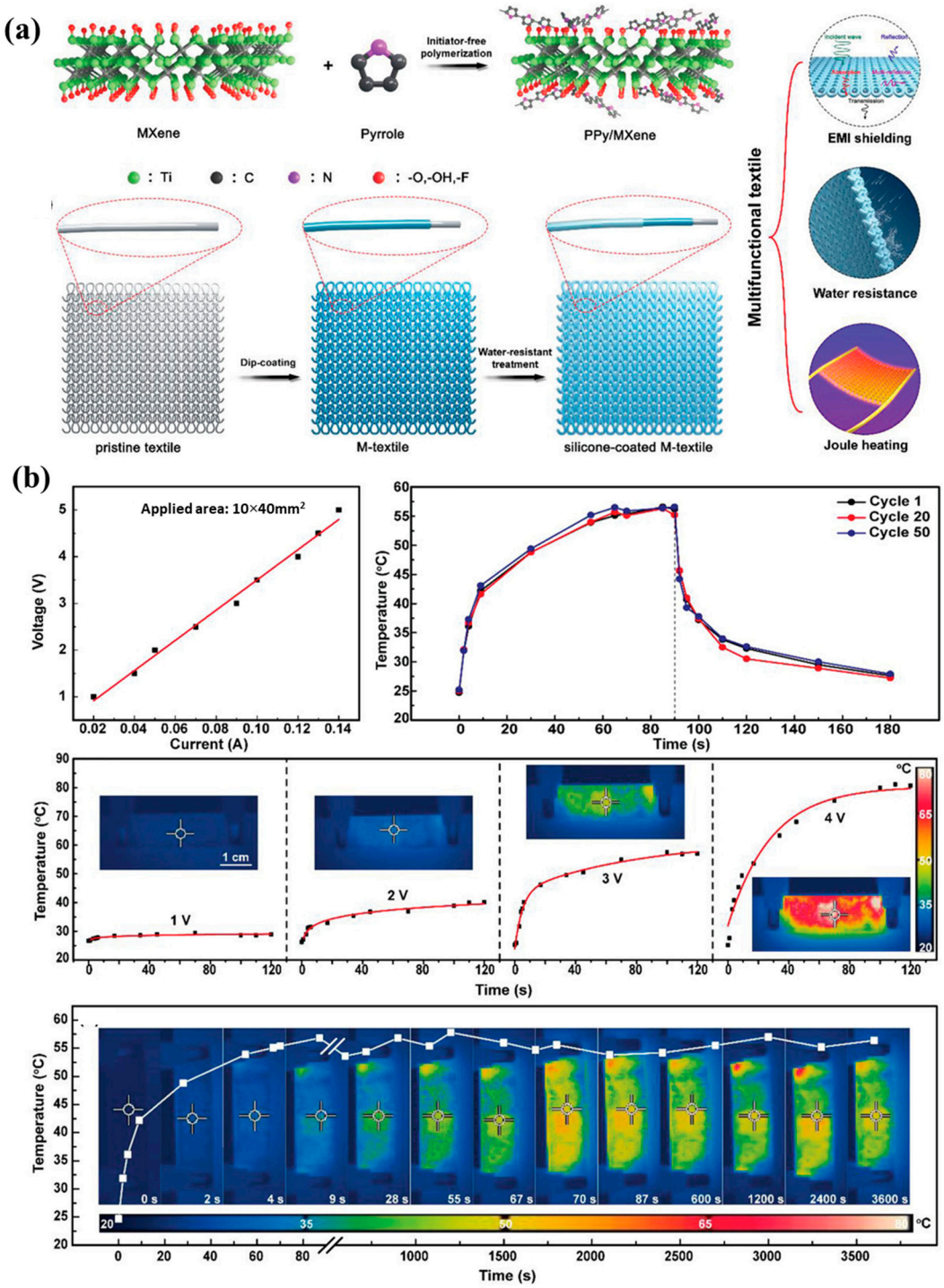

Figure 12. (**a**) Schematic illustrating MXene with in situ polymerized PPy, and its fabrication of PPy/MXene-decorated PET textile and the multifunctional silicone-coated M-textile. (**b**) I–V curve with Joule heating performances of silicone-coated M-textile and time–temperature curve at a constant voltage of 3 V for silicone-coated M-textile [120].

5.5. Solar Water Desalination Applications

A promising approach to mitigate freshwater scarcity is the utilization of solar water desalination. The implementation of photothermal materials at the air–water interface, capable of capturing solar energy and transforming it into thermal energy, has recently been employed to generate interfacial solar steam. This method can implement localized solar desalination, increasing the effectiveness of freshwater collection and seawater evaporation, as displayed in Figure 13a [126]. MXene materials have been demonstrated as a viable alternative to conventional methods for solar desalination due to their higher photothermal conversion efficiency, as reported in the literature [127,128]. A study by Zhao et al. [129] investigated the creation of a hydrophobic MXene composite membrane by modifying a commercial filter membrane with a salt-blocking MXene NSs layer functionalized with trimethoxy (1H,1H,2H,2H-perfluorodecyl) silane. The resulting MXene composite membrane exhibited excellent light utilization, a large number of evaporation channels, and rapid water transport, leading to sustained photothermal transduction under one sun illumination for 200 h. The MXene composite membrane achieved a solar steam conversion efficiency of 71% and a solar evaporation rate of 1.31 kg m^{-2} h^{-1} (Figure 13b,c) [129]. Additionally, the composite membrane's hydrophobic surface could guarantee that materials would be heated directly rather than through water, which was advantageous for maintaining membrane structure and preventing salt from accumulating. After sun evaporation, the seawater could be made to satisfy drinking standards by the MXene composite membrane, which could reject 99.5% of the four primary ions (Mg^{2+}, K^+, Na^+, and Ca^{2+}) present in the seawater, respectively.

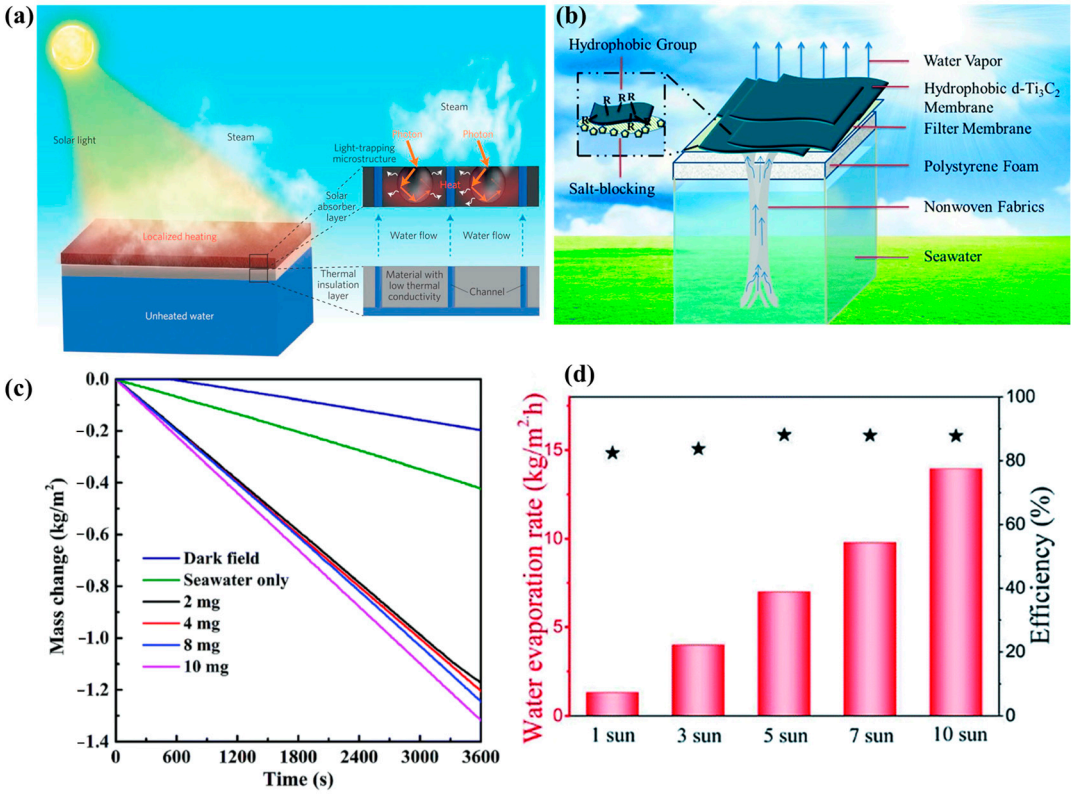

Figure 13. (**a**) Illustration of the representative DSSG process, including a solar absorber layer, a thermal insulator layer, and water transport channels [126]. (**b**,**c**) Schematic of the hydrophobic Ti_3C_2 membrane-based solar desalination device and real-time seawater weight loss through the evaporation of the hydrophobic D-Ti_3C_2 membrane with different loading masses [129]. (**d**) Water evaporation rates (left-hand side axis) and the corresponding solar steam efficiencies of the 3DMA-5 system under solar illumination of different intensities [127].

Furthermore, Zhao et al. [127] constructed a three-dimensional MXene architecture-based solar steam generator, demonstrating a highly efficient steam generation capability. The design process involved a simplified two-step dip coating method and resulted in a material with 98% absorption capacity. The cost-effective and user-friendly composite material was exposed to solar radiation at intensities of one and five suns, resulting in evaporation rates of 1.41 kg/m^2h and 7.49 kg/m^2h, respectively. As illustrated in Figure 13d, the solar steam conversion efficiency was observed to be 88.7% and 94.2% at one and five sun intensities, respectively.

6. Challenges and Future Perspectives

MXene has established itself as a superior 2D material in thermal energy applications, outperforming traditional 2D materials. Its exceptional properties, such as high electrical/thermal conductivity, high light absorptivity, and low infrared emissivity, make it the most promising material for photo-/electrothermal conversion and thermal radiation management. Moreover, the high surface area of MXene provides large interfaces for energy transfer, and the two-dimensional structure allows for fast energy exchange between the solid and liquid phases. As a result, the use of MXene in areas, such as thermal energy usage, personal thermal management, heat dissipation in electronics, and military camouflage, will greatly benefit from its exceptional thermal properties. Although much progress has been made, there are a number of challenges that still need to be overcome before MXene-based thermal materials can be fully utilized in real-world applications. Some of the pressing challenges and future perspectives are listed below:

- Due to technical difficulties and limitations in the synthesis and etching process, only 20 out of 70 MAX phases have been successfully etched into 2D MXene materials. Their inherent properties influence the success and ease of converting MAX phases into 2D MXene materials. Additionally, a lack of understanding or limited research on some MAX phases may impede their successful transformation into 2D MXene materials. The research focus and priority in this area may also be directed towards certain MAX phases due to their specific applications or desired properties.
- Different methods have been used to determine the properties of MXene, and numerous characterization methods have been used to test its stability, strength, and surface characteristics. Phase change materials and nanofluids have effectively used these 2D materials to boost system performance.
- Nanofluids and PCMs with MXene bases showed exceptional optical characteristics and a higher value of "k". Researchers have noted great outcomes from the practical use of these materials in seawater desalination.
- MXene materials exhibit thermal conductivity properties similar to those of ceramics and metals, both known for their high heat conductivity. Theoretical calculations have substantiated the high thermal conductivity potential of MXene materials. However, when considering macroscopic MXene materials such as films, their actual thermal conductivity is lower than expected. To realize the full potential of MXene materials in real-world applications, significant progress must be made in overcoming the challenge of producing macroscopic MXene materials with high thermal conductivity. This requires addressing two crucial scientific issues: controlling the surface termination of MXene and reducing the thermal resistance at the interface between MXene nanosheets during the construction process of macroscopic materials.
- The majority of MXene-based transition metal materials exhibit inadequate mechanical properties, which significantly hinders their utilization in various domains. The viability of MXene-based TM materials as a practical material solution is contingent on enhancing their mechanical properties, including tensile and compressive strength, as well as toughness.
- Although MXene has been widely developed recently, and its applications in the energy sector, particularly in the field of thermal energy, have expanded, it still has some problems that need to be resolved by researchers in the future. Among the principal

obstacles are that the processing of MXene requires secure synthesis pathways that lead to effective, affordable, high-quality, and recurring MXene. Future research must examine the identification of new MAX phases and the related 2D materials. Therefore, future 2D materials with low economic cost and good stability must be considered.

- MXene's limited electrochemical stability restricts its applicability and necessitates more research. However, the high price of MXene-based energy storage materials still poses a significant barrier to progress. Roadblocks related to cost and scale-up can be removed to bring about an energy sector revolution.
- There is a limited understanding of the thermal behavior of MXene-based PCMs. While it is known that MXene-based PCMs have the potential to store and release large amounts of energy, the mechanisms behind this behavior are not yet fully understood. This knowledge gap makes it difficult to predict the performance of MXene-based PCMs under different conditions and to design materials with specific properties.
- MXene-based PCMs have shown great potential for solar energy storage, where they can store excess energy generated by solar panels during the day and release it at night. This can help to reduce the dependence on grid-connected power and improve the overall efficiency of solar energy systems. In addition, MXene-based PCMs can be used to regulate the temperature of solar panels, increasing their efficiency and lifespan.
- In thermal energy storage, MXene-based PCMs can be used to store and release heat generated by industrial processes, heating and cooling systems, and renewable energy sources. They can provide stable and efficient temperature control, reducing energy waste and increasing the efficiency of energy systems. In addition, the high thermal stability of MXene-based PCMs allows for multiple phase transitions without degradation, making them suitable for long-term energy storage.
- Its application areas should be increased in order to increase the use of MXene in research and development fields, particularly thermal management.

7. Conclusions

MXene-based phase change materials have enormous potential for solar and thermal energy applications. Their superior electrical and thermal conductivity, high thermal energy storage density, and high thermal stability make them a promising alternative to traditional PCMs. However, further research and development are required to overcome scalability and compatibility challenges and bring MXene-based PCMs to market. With continued investment and collaboration between academia, industry, and government, MXene-based PCMs will likely play an essential role in the future of energy storage and sustainable energy systems. The future prospects of MXene-based PCMs are promising, and they have the potential to revolutionize the energy storage and thermal management industries.

Funding: The authors thank Xiamen University for awarding the Research Fund (XMUMRF/C6IENG/0030) and Sunway University for the Rewarding Research Output grant (GRTIN-RRO-60-2022) for this work.

Institutional Review Board Statement: Not applicable.

Informed Consent Statement: Not applicable.

Data Availability Statement: Data is contained within the article.

Conflicts of Interest: The authors declare no conflict of interest.

References

1. Yin, X.; Yang, R.; Tan, G.; Fan, S. Terrestrial radiative cooling: Using the cold universe as a renewable and sustainable energy source. *Science* **2020**, *370*, 786–791. [CrossRef]
2. Ying, J.; Tan, X.; Lv, L.; Wang, X.; Gao, J.; Yan, Q.; Ma, H.; Nishimura, K.; Li, H.; Yu, J. Tailoring highly ordered graphene framework in epoxy for high-performance polymer-based heat dissipation plates. *ACS Nano* **2021**, *15*, 12922–12934. [CrossRef]

3. Ye, Y.; Chou, L.-Y.; Liu, Y.; Wang, H.; Lee, H.K.; Huang, W.; Wan, J.; Liu, K.; Zhou, G.; Yang, Y. Ultralight and fire-extinguishing current collectors for high-energy and high-safety lithium-ion batteries. *Nat. Energy* **2020**, *5*, 786–793. [CrossRef]
4. Hu, R.; Liu, Y.; Shin, S.; Huang, S.; Ren, X.; Shu, W.; Cheng, J.; Tao, G.; Xu, W.; Chen, R. Emerging materials and strategies for personal thermal management. *Adv. Energy Mater.* **2020**, *10*, 1903921. [CrossRef]
5. Han, C.-G.; Qian, X.; Li, Q.; Deng, B.; Zhu, Y.; Han, Z.; Zhang, W.; Wang, W.; Feng, S.-P.; Chen, G. Giant thermopower of ionic gelatin near room temperature. *Science* **2020**, *368*, 1091–1098. [CrossRef]
6. Benyettou, F.; Das, G.; Nair, A.R.; Prakasam, T.; Shinde, D.B.; Sharma, S.K.; Whelan, J.; Lalatonne, Y.; Traboulsi, H.; Pasricha, R. Covalent organic framework embedded with magnetic nanoparticles for MRI and chemo-thermotherapy. *J. Am. Chem. Soc.* **2020**, *142*, 18782–18794. [CrossRef]
7. Ding, T.; Zhou, Y.; Ong, W.L.; Ho, G.W. Hybrid solar-driven interfacial evaporation systems: Beyond water production towards high solar energy utilization. *Mater. Today* **2021**, *42*, 178–191. [CrossRef]
8. Hu, R.; Xi, W.; Liu, Y.; Tang, K.; Song, J.; Luo, X.; Wu, J.; Qiu, C.-W. Thermal camouflaging metamaterials. *Mater. Today* **2021**, *45*, 120–141. [CrossRef]
9. Bark, H.; Tan, M.W.M.; Thangavel, G.; Lee, P.S. Deformable high loading liquid metal nanoparticles composites for thermal energy management. *Adv. Energy Mater.* **2021**, *11*, 2101387. [CrossRef]
10. Xu, Y.; Kraemer, D.; Song, B.; Jiang, Z.; Zhou, J.; Loomis, J.; Wang, J.; Li, M.; Ghasemi, H.; Huang, X. Nanostructured polymer films with metal-like thermal conductivity. *Nat. Commun.* **2019**, *10*, 1–8. [CrossRef]
11. Yan, Q.; Dai, W.; Gao, J.; Tan, X.; Lv, L.; Ying, J.; Lu, X.; Lu, J.; Yao, Y.; Wei, Q. Ultrahigh-aspect-ratio boron nitride nanosheets leading to superhigh in-plane thermal conductivity of foldable heat spreader. *ACS Nano* **2021**, *15*, 6489–6498. [CrossRef]
12. He, S.; Li, Y.; Liu, L.; Jiang, Y.; Feng, J.; Zhu, W.; Zhang, J.; Dong, Z.; Deng, Y.; Luo, J. Semiconductor glass with superior flexibility and high room temperature thermoelectric performance. *Sci. Adv.* **2020**, *6*, eaaz8423. [CrossRef]
13. Zhuang, Y.; Zheng, K.; Cao, X.; Fan, Q.; Ye, G.; Lu, J.; Zhang, J.; Ma, Y. Flexible graphene nanocomposites with simultaneous highly anisotropic thermal and electrical conductivities prepared by engineered graphene with flat morphology. *ACS Nano* **2020**, *14*, 11733–11742. [CrossRef]
14. Lewis, N.S. Toward cost-effective solar energy use. *Science* **2007**, *315*, 798–801. [CrossRef]
15. Regin, A.F.; Solanki, S.; Saini, J. Heat transfer characteristics of thermal energy storage system using PCM capsules: A review. *Renew. Sustain. Energy Rev.* **2008**, *12*, 2438–2458. [CrossRef]
16. Kaygusuz, K. The viability of thermal energy storage. *Energy Sources* **1999**, *21*, 745–755. [CrossRef]
17. Sharma, A.; Tyagi, V.V.; Chen, C.R.; Buddhi, D. Review on thermal energy storage with phase change materials and applications. *Renew. Sustain. Energy Rev.* **2009**, *13*, 318–345. [CrossRef]
18. Telkes, M.; Raymond, E. Storing solar heat in chemicals. *Heat. Vent.* **1949**, *46*, 80–86.
19. Pielichowska, K.; Pielichowski, K. Phase change materials for thermal energy storage. *Prog. Mater. Sci.* **2014**, *65*, 67–123. [CrossRef]
20. Kenisarin, M.; Mahkamov, K. Solar energy storage using phase change materials. *Renew. Sustain. Energy Rev.* **2007**, *11*, 1913–1965. [CrossRef]
21. Fernandes, D.; Pitié, F.; Cáceres, G.; Baeyens, J. Thermal energy storage: "How previous findings determine current research priorities". *Energy* **2012**, *39*, 246–257. [CrossRef]
22. Garg, H.; Mullick, S.; Bhargava, A. Latent heat or phase change thermal energy storage. In *Solar Thermal Energy Storage*; Springer: Berlin/Heidelberg, Germany, 1985; pp. 154–291.
23. Hasnain, S. Review on sustainable thermal energy storage technologies, Part I: Heat storage materials and techniques. *Energy Convers. Manag.* **1998**, *39*, 1127–1138. [CrossRef]
24. Selamat, U.; Osman, K.; Rahim, A.H.A. Heat and Flow Analysis of a Chilled Water Storage System using Computational Fluid Dynamics. *J. Adv. Res. Fluid Mech. Therm. Sci.* **2019**, *57*, 131–140.
25. Rashid, F.L.; Shareef, A.S.; Alwan, H.F. Enhancement of fresh water production in solar still using new phase change materials. *J. Adv. Res. Fluid Mech. Therm. Sci.* **2019**, *61*, 63–72.
26. Krishna, Y.; Faizal, M.; Saidur, R.; Ng, K.; Aslfattahi, N. State-of-the-art heat transfer fluids for parabolic trough collector. *Int. J. Heat Mass Transf.* **2020**, *152*, 119541. [CrossRef]
27. Krishna, Y.; Aslfattahi, N.; Saidur, R.; Faizal, M.; Ng, K. Fatty acid/metal ion composite as thermal energy storage materials. *SN Appl. Sci.* **2020**, *2*, 1–10. [CrossRef]
28. Zendehboudi, A.; Aslfattahi, N.; Rahman, S.; Sabri, M.F.M.; Said, S.M.; Arifutzzaman, A.; Sidik, N.A.C. Optimization of thermal conductivity of NanoPCM-based graphene by response surface methodology. *J. Adv. Res. Fluid Mech. Therm. Sci.* **2020**, *75*, 108–125.
29. Novoselov, K.S.; Geim, A.K.; Morozov, S.V.; Jiang, D.-e.; Zhang, Y.; Dubonos, S.V.; Grigorieva, I.V.; Firsov, A.A. Electric field effect in atomically thin carbon films. *Science* **2004**, *306*, 666–669. [CrossRef]
30. Pacile, D.; Meyer, J.; Girit, Ç.; Zettl, A. The two-dimensional phase of boron nitride: Few-atomic-layer sheets and suspended membranes. *Appl. Phys. Lett.* **2008**, *92*, 133107. [CrossRef]
31. Ataca, C.; Sahin, H.; Ciraci, S. Stable, Single-Layer MX_2 Transition-Metal Oxides and Dichalcogenides in a Honeycomb-Like Structure. *J. Phys. Chem. C* **2012**, *116*, 8983–8999. [CrossRef]
32. Naguib, M.; Kurtoglu, M.; Presser, V.; Lu, J.; Niu, J.; Heon, M.; Hultman, L.; Gogotsi, Y.; Barsoum, M.W. Two-dimensional nanocrystals produced by exfoliation of Ti_3AlC_2. *Adv. Mater.* **2011**, *23*, 4248–4253. [CrossRef]

33. Naguib, M.; Gogotsi, Y. Synthesis of two-dimensional materials by selective extraction. *Acc. Chem. Res.* **2015**, *48*, 128–135. [CrossRef] [PubMed]
34. Parashar, N.; Aslfattahi, N.; Yahya, S.M.; Saidur, R. An artificial neural network approach for the prediction of dynamic viscosity of MXene-palm oil nanofluid using experimental data. *J. Therm. Anal. Calorim.* **2021**, *144*, 1175–1186. [CrossRef]
35. Aslfattahi, N.; Saidur, R.; Arifutzzaman, A.; Sadri, R.; Bimbo, N.; Sabri, M.F.M.; Maughan, P.A.; Bouscarrat, L.; Dawson, R.J.; Said, S.M. Experimental investigation of energy storage properties and thermal conductivity of a novel organic phase change material/MXene as A new class of nanocomposites. *J. Energy Storage* **2020**, *27*, 101115. [CrossRef]
36. Numan, A.; Rafique, S.; Khalid, M.; Zaharin, H.A.; Radwan, A.; Mokri, N.A.; Ching, O.P.; Walvekar, R. Microwave-assisted rapid MAX phase etching and delamination: A paradigm shift in MXene synthesis. *Mater. Chem. Phys.* **2022**, *288*, 126429. [CrossRef]
37. Khosla, A.; Awan, H.T.A.; Singh, K.; Walvekar, R.; Zhao, Z.; Kaushik, A.; Khalid, M.; Chaudhary, V. Emergence of MXene and MXene–Polymer Hybrid Membranes as Future-Environmental Remediation Strategies. *Adv. Sci.* **2022**, *9*, 2203527. [CrossRef]
38. Rasool, K.; Pandey, R.P.; Rasheed, P.A.; Buczek, S.; Gogotsi, Y.; Mahmoud, K.A. Water treatment and environmental remediation applications of two-dimensional metal carbides (MXenes). *Mater. Today* **2019**, *30*, 80–102. [CrossRef]
39. Huang, K.; Li, Z.; Lin, J.; Han, G.; Huang, P. Two-dimensional transition metal carbides and nitrides (MXenes) for biomedical applications. *Chem. Soc. Rev.* **2018**, *47*, 5109–5124. [CrossRef]
40. Chaudhary, V.; Khanna, V.; Awan, H.T.A.; Singh, K.; Khalid, M.; Mishra, Y.; Bhansali, S.; Li, C.-Z.; Kaushik, A. Towards hospital-on-chip supported by 2D MXenes-based 5th generation intelligent biosensors. *Biosens. Bioelectron.* **2022**, *220*, 114847. [CrossRef]
41. Barsoum, M.W. *MAX Phases: Properties of Machinable Ternary Carbides and Nitrides*; John Wiley & Sons: Hoboken, NJ, USA, 2013.
42. Verger, L.; Xu, C.; Natu, V.; Cheng, H.-M.; Ren, W.; Barsoum, M.W. Overview of the synthesis of MXenes and other ultrathin 2D transition metal carbides and nitrides. *Curr. Opin. Solid State Mater. Sci.* **2019**, *23*, 149–163. [CrossRef]
43. Nowotny, V.H. Strukturchemie einiger verbindungen der übergangsmetalle mit den elementen C, Si, Ge, Sn. *Prog. Solid State Chem.* **1971**, *5*, 27–70. [CrossRef]
44. Anasori, B.; Halim, J.; Lu, J.; Voigt, C.A.; Hultman, L.; Barsoum, M.W. Mo_2TiAlC_2: A new ordered layered ternary carbide. *Scr. Mater.* **2015**, *101*, 5–7. [CrossRef]
45. Tao, Q.; Dahlqvist, M.; Lu, J.; Kota, S.; Meshkian, R.; Halim, J.; Palisaitis, J.; Hultman, L.; Barsoum, M.W.; Persson, P.O. Two-dimensional Mo1. 33C MXene with divacancy ordering prepared from parent 3D laminate with in-plane chemical ordering. *Nat. Commun.* **2017**, *8*, 14949. [CrossRef] [PubMed]
46. Tao, Q.; Lu, J.; Dahlqvist, M.; Mockute, A.; Calder, S.; Petruhins, A.; Meshkian, R.; Rivin, O.; Potashnikov, D.; Caspi, E.a.N. Atomically layered and ordered rare-earth i-MAX phases: A new class of magnetic quaternary compounds. *Chem. Mater.* **2019**, *31*, 2476–2485. [CrossRef]
47. Anasori, B.; Lukatskaya, M.R.; Gogotsi, Y. 2D metal carbides and nitrides (MXenes) for energy storage. *Nat. Rev. Mater.* **2017**, *2*, 1–17. [CrossRef]
48. Cambaz, G.Z.; Yushin, G.N.; Gogotsi, Y.; Lutsenko, V.G. Anisotropic etching of SiC whiskers. *Nano Lett.* **2006**, *6*, 548–551. [CrossRef]
49. Seh, Z.W.; Fredrickson, K.D.; Anasori, B.; Kibsgaard, J.; Strickler, A.L.; Lukatskaya, M.R.; Gogotsi, Y.; Jaramillo, T.F.; Vojvodic, A. Two-dimensional molybdenum carbide (MXene) as an efficient electrocatalyst for hydrogen evolution. *ACS Energy Lett.* **2016**, *1*, 589–594. [CrossRef]
50. Ghidiu, M.; Lukatskaya, M.R.; Zhao, M.-Q.; Gogotsi, Y.; Barsoum, M.W. Conductive two-dimensional titanium carbide 'clay'with high volumetric capacitance. *Nature* **2014**, *516*, 78–81. [CrossRef]
51. Alhabeb, M.; Maleski, K.; Anasori, B.; Lelyukh, P.; Clark, L.; Sin, S.; Gogotsi, Y. Guidelines for synthesis and processing of two-dimensional titanium carbide ($Ti_3C_2T_x$ MXene). *Chem. Mater.* **2017**, *29*, 7633–7644. [CrossRef]
52. Hu, S.; Li, S.; Xu, W.; Zhang, J.; Zhou, Y.; Cheng, Z. Rapid preparation, thermal stability and electromagnetic interference shielding properties of two-dimensional Ti_3C_2 MXene. *Ceram. Int.* **2019**, *45*, 19902–19909. [CrossRef]
53. Mashtalir, O.; Naguib, M.; Mochalin, V.N.; Dall'Agnese, Y.; Heon, M.; Barsoum, M.W.; Gogotsi, Y. Intercalation and delamination of layered carbides and carbonitrides. *Nat. Commun.* **2013**, *4*, 1–7. [CrossRef] [PubMed]
54. Ghidiu, M.; Halim, J.; Kota, S.; Bish, D.; Gogotsi, Y.; Barsoum, M.W. Ion-exchange and cation solvation reactions in Ti_3C_2 MXene. *Chem. Mater.* **2016**, *28*, 3507–3514. [CrossRef]
55. Natu, V.; Sokol, M.; Verger, L.; Barsoum, M.W. Effect of Edge Charges on Stability and Aggregation of $Ti_3C_2T_z$ MXene Colloidal Suspensions. *J. Phys. Chem. C* **2018**, *122*, 27745–27753. [CrossRef]
56. Omomo, Y.; Sasaki, T.; Wang, L.; Watanabe, M. Redoxable nanosheet crystallites of MnO_2 derived via delamination of a layered manganese oxide. *J. Am. Chem. Soc.* **2003**, *125*, 3568–3575. [CrossRef] [PubMed]
57. Nickl, J.J.; Schweitzer, K.K.; Luxenberg, P. Gasphasenabscheidung im system Ti Si C. *J. Less Common Met.* **1972**, *26*, 335–353. [CrossRef]
58. Yin, X.; Travitzky, N.; Greil, P. Three-dimensional printing of nanolaminated Ti_3AlC_2 toughened $TiAl_3$–Al_2O_3 composites. *J. Am. Ceram. Soc.* **2007**, *90*, 2128–2134. [CrossRef]
59. Xu, C.; Wang, L.; Liu, Z.; Chen, L.; Guo, J.; Kang, N.; Ma, X.-L.; Cheng, H.-M.; Ren, W. Large-area high-quality 2D ultrathin Mo2C superconducting crystals. *Nat. Mater.* **2015**, *14*, 1135–1141. [CrossRef]

60. Yang, C.; Jiang, Q.; Li, W.; He, H.; Yang, L.; Lu, Z.; Huang, H. Ultrafine Pt nanoparticle-decorated 3D hybrid architectures built from reduced graphene oxide and MXene nanosheets for methanol oxidation. *Chem. Mater.* **2019**, *31*, 9277–9287. [CrossRef]
61. Yang, C.; Jiang, Q.; Huang, H.; He, H.; Yang, L.; Li, W. Polyelectrolyte-Induced Stereoassembly of Grain Boundary-Enriched Platinum Nanoworms on $Ti_3C_2T_x$ MXene Nanosheets for Efficient Methanol Oxidation. *ACS Appl. Mater. Interfaces* **2020**, *12*, 23822–23830. [CrossRef]
62. Wang, Z.; Kochat, V.; Pandey, P.; Kashyap, S.; Chattopadhyay, S.; Samanta, A.; Sarkar, S.; Manimunda, P.; Zhang, X.; Asif, S. Metal immiscibility route to synthesis of ultrathin carbides, borides, and nitrides. *Adv. Mater.* **2017**, *29*, 1700364. [CrossRef]
63. Jia, J.; Xiong, T.; Zhao, L.; Wang, F.; Liu, H.; Hu, R.; Zhou, J.; Zhou, W.; Chen, S. Ultrathin N-doped Mo2C nanosheets with exposed active sites as efficient electrocatalyst for hydrogen evolution reactions. *ACS Nano* **2017**, *11*, 12509–12518. [CrossRef] [PubMed]
64. Fan, X.; Liu, L.; Jin, X.; Wang, W.; Zhang, S.; Tang, B. MXene $Ti_3C_2T_x$ for phase change composite with superior photothermal storage capability. *J. Mater. Chem. A* **2019**, *7*, 14319–14327. [CrossRef]
65. Joshi, S.; Wang, Q.; Puntambekar, A.; Chakrapani, V. Facile synthesis of large area two-dimensional layers of transition-metal nitride and their use as insertion electrodes. *ACS Energy Lett.* **2017**, *2*, 1257–1262. [CrossRef]
66. Zhang, F.; Zhang, Z.; Wang, H.; Chan, C.H.; Chan, N.Y.; Chen, X.X.; Dai, J.-Y. Plasma-enhanced pulsed-laser deposition of single-crystalline Mo_2C ultrathin superconducting films. *Phys. Rev. Mater.* **2017**, *1*, 034002. [CrossRef]
67. Zhang, Z.; Zhang, F.; Wang, H.; Chan, C.H.; Lu, W.; Dai, J.-y. Substrate orientation-induced epitaxial growth of face centered cubic Mo_2C superconductive thin film. *J. Mater. Chem. C* **2017**, *5*, 10822–10827. [CrossRef]
68. Zalba, B.; Marín, J.M.; Cabeza, L.F.; Mehling, H. Review on thermal energy storage with phase change: Materials, heat transfer analysis and applications. *Appl. Therm. Eng.* **2003**, *23*, 251–283. [CrossRef]
69. Cabeza, L.F.; Castell, A.; Barreneche, C.; De Gracia, A.; Fernández, A.I. Materials used as PCM in thermal energy storage in buildings: A review. *Renew. Sustain. Energy Rev.* **2011**, *15*, 1675–1695. [CrossRef]
70. Oró, E.; Barreneche, C.; Farid, M.M.; Cabeza, L.F. Experimental study on the selection of phase change materials for low temperature applications. *Renew. Energy* **2013**, *57*, 130–136. [CrossRef]
71. Singh, S.; Gaikwad, K.K.; Lee, Y.S. Phase change materials for advanced cooling packaging. *Environ. Chem. Lett.* **2018**, *16*, 845–859. [CrossRef]
72. Hasan, A.; McCormack, S.J.; Huang, M.J.; Norton, B. Evaluation of phase change materials for thermal regulation enhancement of building integrated photovoltaics. *Sol. Energy* **2010**, *84*, 1601–1612. [CrossRef]
73. Huang, M.J. The effect of using two PCMs on the thermal regulation performance of BIPV systems. *Sol. Energy Mater. Sol. Cells* **2011**, *95*, 957–963. [CrossRef]
74. Biwole, P.H.; Eclache, P.; Kuznik, F. Phase-change materials to improve solar panel's performance. *Energy Build.* **2013**, *62*, 59–67. [CrossRef]
75. Lo, B.V.; Ciulla, G.; Piacentino, A.; Cardona, F. On the efficacy of PCM to shave peak temperature of crystalline photovoltaic panels: An FDM model and field validation. *Energies* **2013**, *6*, 6188–6210.
76. Huang, M.J.; Eames, P.C.; Norton, B.; Hewitt, N.J. Natural convection in an internally finned phase change material heat sink for the thermal management of photovoltaics. *Sol. Energy Mater. Sol. Cells* **2011**, *95*, 1598–1603. [CrossRef]
77. Hendricks, J.H.C.; Sark, W.G.J.H.M. Annual performance enhancement of building integrated photovoltaic modules by applying phase change materials. *Prog. Photovolt.* **2013**, *21*, 620–630. [CrossRef]
78. Sharma, S.; Tahir, A.; Reddy, K.S.; Mallick, T.K. Performance enhancement of a Building-Integrated Concentrating Photovoltaic system using phase change material. *Sol. Energy Mater. Sol. Cells* **2016**, *149*, 29–39. [CrossRef]
79. Pakrouh, R.; Hosseini, M.J.; Ranjbar, A.A. A parametric investigation of a PCM-based pin fin heat sink. *Mech. Sci.* **2015**, *6*, 65–73. [CrossRef]
80. Machniewicz, A.; Knera, D.; Heim, D. Effect of Transition Temperature on Efficiency of PV/PCM Panels. *Energy Procedia* **2015**, *78*, 1684–1689. [CrossRef]
81. Javani, N.; Dincer, I.; Naterer, G.F. New latent heat storage system with nanoparticles for thermal management of electric vehicles. *J. Power Sources* **2014**, *268*, 718–727. [CrossRef]
82. Khodadadi, J.M.; Hosseinizadeh, S.F. Nanoparticle-enhanced phase change materials (NEPCM) with great potential for improved thermal energy storage. *Int. Commun. Heat Mass Transf.* **2007**, *34*, 534–543. [CrossRef]
83. Kant, K.; Shukla, A.; Sharma, A.; Henry Biwole, P. Heat transfer study of phase change materials with graphene nano particle for thermal energy storage. *Sol. Energy* **2017**, *146*, 453–463. [CrossRef]
84. Ho, C.J.; Gao, J.Y. Preparation and thermophysical properties of nanoparticle-in-paraffin emulsion as phase change material. *Int. Commun. Heat Mass Transf.* **2009**, *36*, 467–470. [CrossRef]
85. Hajare, V.; Gawali, B. Experimental study of latent heat storage system using nano-mixed phase change material. *Int. J. Eng. Technol. Manag. Ment Appl. Sci.* **2015**, *3*, 37–44.
86. Hajare, V.; Narode, A.; Gawali, B.; Bamane, S. Technology. Experimental investigation of enhancement in heat transfer using nano-mixed PCM. *Int. J. Eng. Res.* **2014**, *3*, 843–848.
87. Ab Latif, F.E.; Numan, A.; Mubarak, N.M.; Khalid, M.; Abdullah, E.C.; Manaf, N.A. Walvekar, REvolution of MXene and its 2D heterostructure in electrochemical sensor applications. *Co-Ord. Chem. Rev.* **2022**, *471*, 214755. [CrossRef]

88. Raheem, I.; Mubarak, N.M.; Karri, R.R.; Solangi, N.H.; Jatoi, A.S.; Mazari, S.A.; Khalid, M.; Tan, Y.H.; Koduru, J.R.; Malafaia, G.J.C. Rapid growth of MXene-based membranes for sustainable environmental pollution remediation. *Chemosphere* **2022**, *311*, 137056. [CrossRef]
89. Kailasa, S.K.; Joshi, D.J.; Koduru, J.R.; Malek, N.I. Review on MXenes-based nanomaterials for sustainable opportunities in energy storage, sensing and electrocatalytic reactions. *J. Mol. Liq.* **2021**, *342*, 117524. [CrossRef]
90. Hantanasirisakul, K.; Zhao, M.Q.; Urbankowski, P.; Halim, J.; Anasori, B.; Kota, S.; Ren, C.E.; Barsoum, M.W.; Gogotsi, Y. Fabrication of $Ti_3C_2T_x$ MXene transparent thin films with tunable optoelectronic properties. *Adv. Eletron. Mater.* **2016**, *2*, 1600050. [CrossRef]
91. Halim, J.; Lukatskaya, M.R.; Cook, K.M.; Lu, J.; Smith, C.R.; Näslund, L.-Å.; May, S.J.; Hultman, L.; Gogotsi, Y.; Eklund, P.; et al. Transparent Conductive Two-Dimensional Titanium Carbide Epitaxial Thin Films. *Chem. Mater.* **2014**, *26*, 2374–2381. [CrossRef]
92. Wassei, J.K.; Kaner, R.B. Graphene, a promising transparent conductor. *Mater. Today* **2010**, *13*, 52–59. [CrossRef]
93. Becerril, H.A.; Mao, J.; Liu, Z.; Stoltenberg, R.M.; Bao, Z.; Chen, Y. Evaluation of solution-processed reduced graphene oxide films as transparent conductors. *ACS Nano* **2008**, *2*, 463–470. [CrossRef] [PubMed]
94. Wang, X.; Yu, W.; Wang, L.; Xie, H. Vertical orientation graphene/MXene hybrid phase change materials with anisotropic properties, high enthalpy, and photothermal conversion. *Sci. China Technol. Sci.* **2022**, *65*, 882–892. [CrossRef]
95. Liu, H.; Fu, R.; Su, X.; Wu, B.; Wang, H.; Xu, Y.; Liu, X. MXene confined in shape-stabilized phase change material combining enhanced electromagnetic interference shielding and thermal management capability. *Compos. Sci. Technol.* **2021**, *210*, 108835. [CrossRef]
96. Du, Y.; Huang, H.; Hu, X.; Liu, S.; Sheng, X.; Li, X.; Lu, X.; Qu, J. Melamine foam/polyethylene glycol composite phase change material synergistically modified by polydopamine/MXene with enhanced solar-to-thermal conversion. *Renew. Energy* **2021**, *171*, 1–10. [CrossRef]
97. Wang, F.; Guo, J.; Li, S.; Wang, Y.; Hu, X.; Li, Z.; Shen, Y.; Li, C. Facile self-assembly approach to construct a novel MXene-decorated nano-sized phase change material emulsion for thermal energy storage. *Ceram. Int.* **2022**, *48*, 4722–4731. [CrossRef]
98. Sheng, X.; Dong, D.; Lu, X.; Zhang, L.; Chen, Y. MXene-wrapped bio-based pomelo peel foam/polyethylene glycol composite phase change material with enhanced light-to-thermal conversion efficiency, thermal energy storage capability and thermal conductivity. *Compos. Part A Appl. Sci. Manuf.* **2020**, *138*, 106067. [CrossRef]
99. Khan, A.A.; Yahya, S.M.; Ali, M.A. Synthesis and Characterization of Titania–MXene-Based Phase Change Material for Sustainable Thermal Energy Storage. *Sustainability* **2023**, *15*, 516. [CrossRef]
100. Luo, Y.; Xie, Y.; Jiang, H.; Chen, Y.; Zhang, L.; Sheng, X.; Xie, D.; Wu, H.; Mei, Y. Flame-retardant and form-stable phase change composites based on MXene with high thermostability and thermal conductivity for thermal energy storage. *Chem. Eng. J.* **2021**, *420*, 130466. [CrossRef]
101. Cheng, H.; Xing, L.; Zuo, Y.; Pan, Y.; Huang, M.; Alhadhrami, A.; Ibrahim, M.M.; El-Bahy, Z.M.; Liu, C.; Shen, C.; et al. Constructing nickel chain/MXene networks in melamine foam towards phase change materials for thermal energy management and absorption-dominated electromagnetic interference shielding. *Adv. Compos. Hybrid Mater.* **2022**, *5*, 755–765. [CrossRef]
102. Shao, Y.-W.; Hu, W.-W.; Gao, M.-H.; Xiao, Y.-Y.; Huang, T.; Zhang, N.; Yang, J.-H.; Qi, X.-D.; Wang, Y. Flexible MXene-coated melamine foam based phase change material composites for integrated solar-thermal energy conversion/storage, shape memory and thermal therapy functions. *Compos. Part A Appl. Sci. Manuf.* **2021**, *143*, 106291. [CrossRef]
103. Gao, S.; Ding, J.; Wang, W.; Lu, J. MXene based flexible composite phase change material with shape memory, self-healing and flame retardant for thermal management. *Compos. Sci. Technol.* **2023**, *234*, 109945. [CrossRef]
104. Krishna, Y.; Saidur, R.; Aslfattahi, N.; Faizal, M.; Ng, K. Enhancing the thermal properties of organic phase change material (palmitic acid) by doping MXene nanoflakes. In *AIP Conference Proceedings*; AIP Publishing LLC: Melville, NY, USA, 2020.
105. Wang, L.; Liang, W.; Wang, C.; Fan, Y.; Liu, Y.; Xiao, C.; Sun, H.; Zhu, Z.; Li, A. Dodecylamine/Ti_3C_2-pectin form-stable phase change composites with enhanced light-to-thermal conversion and mechanical properties. *Renew. Energy* **2021**, *176*, 663–674. [CrossRef]
106. Du, X.; Qiu, J.; Deng, S.; Du, Z.; Cheng, X.; Wang, H. $Ti_3C_2T_x$@PDA-Integrated Polyurethane Phase Change Composites with Superior Solar-Thermal Conversion Efficiency and Improved Thermal Conductivity. *ACS Sustain. Chem. Eng.* **2020**, *8*, 5799–5806. [CrossRef]
107. Ji, X.; Jiang, Y.; Liu, T.; Lin, S.; Du, A. MXene aerogel-based phase change film for synergistic thermal management inspired by antifreeze beetles. *Cell Rep. Phys. Sci.* **2022**, *3*, 100815. [CrossRef]
108. Mo, Z.; Mo, P.; Yi, M.; Hu, Z.; Tan, G.; Selim, M.S.; Chen, Y.; Chen, X.; Hao, Z.; Wei, X.; et al. $Ti_3C_2T_x$@ polyvinyl alcohol foam-supported phase change materials with simultaneous enhanced thermal conductivity and solar-thermal conversion performance. *Sol. Energy Mater. Sol. Cells* **2021**, *219*, 110813. [CrossRef]
109. Jiang, X.; Liu, S.; Liang, W.; Luo, S.; He, Z.; Ge, Y.; Wang, H.; Cao, R.; Zhang, F.; Wen, Q. Broadband nonlinear photonics in few-layer MXene $Ti_3C_2T_x$ (T = F, O, or OH). *Laser Photonics Rev.* **2018**, *12*, 1700229. [CrossRef]
110. Lin, P.; Xie, J.; He, Y.; Lu, X.; Li, W.; Fang, J.; Yan, S.; Zhang, L.; Sheng, X.; Chen, Y. MXene aerogel-based phase change materials toward solar energy conversion. *Sol. Energy Mater. Sol. Cells* **2020**, *206*, 110229. [CrossRef]
111. Lu, X.; Huang, H.; Zhang, X.; Lin, P.; Huang, J.; Sheng, X.; Zhang, L.; Qu, J.-p. Novel light-driven and electro-driven polyethylene glycol/two-dimensional MXene form-stable phase change material with enhanced thermal conductivity and electrical conductivity for thermal energy storage. *Compos. Part B Eng.* **2019**, *177*, 107372. [CrossRef]

112. Wang, C.; Wang, Y.; Jiang, X.; Xu, J.; Huang, W.; Zhang, F.; Liu, J.; Yang, F.; Song, Y.; Ge, Y. MXene $Ti_3C_2T_x$: A promising photothermal conversion material and application in all-optical modulation and all-optical information loading. *Adv. Opt. Mater.* **2019**, *7*, 1900060. [CrossRef]
113. Tao, P.; Ni, G.; Song, C.; Shang, W.; Wu, J.; Zhu, J.; Chen, G.; Deng, T. Solar-driven interfacial evaporation. *Nat. Energy* **2018**, *3*, 1031–1041. [CrossRef]
114. Lü, B.; Chen, Y.; Li, P.; Wang, B.; Müllen, K.; Yin, M. Stable radical anions generated from a porous perylenediimide metal-organic framework for boosting near-infrared photothermal conversion. *Nat. Commun.* **2019**, *10*, 1–8. [CrossRef]
115. Lin, K.-T.; Lin, H.; Yang, T.; Jia, B. Structured graphene metamaterial selective absorbers for high efficiency and omnidirectional solar thermal energy conversion. *Nat. Commun.* **2020**, *11*, 1–10. [CrossRef]
116. Wang, C.; Astruc, D. Nanogold plasmonic photocatalysis for organic synthesis and clean energy conversion. *Chem. Soc. Rev.* **2014**, *43*, 7188–7216. [CrossRef]
117. Robinson, J.T.; Tabakman, S.M.; Liang, Y.; Wang, H.; Sanchez Casalongue, H.; Vinh, D.; Dai, H. Ultrasmall reduced graphene oxide with high near-infrared absorbance for photothermal therapy. *J. Am. Chem. Soc.* **2011**, *133*, 6825–6831. [CrossRef]
118. Iqbal, A.; Shahzad, F.; Hantanasirisakul, K.; Kim, M.-K.; Kwon, J.; Hong, J.; Kim, H.; Kim, D.; Gogotsi, Y.; Koo, C.M. Anomalous absorption of electromagnetic waves by 2D transition metal carbonitride Ti_3CNT_x (MXene). *Science* **2020**, *369*, 446–450. [CrossRef]
119. Li, R.; Zhang, L.; Shi, L.; Wang, P. MXene Ti_3C_2: An effective 2D light-to-heat conversion material. *ACS Nano* **2017**, *11*, 3752–3759. [CrossRef]
120. Wang, Q.W.; Zhang, H.B.; Liu, J.; Zhao, S.; Xie, X.; Liu, L.; Yang, R.; Koratkar, N.; Yu, Z.Z. Multifunctional and water-resistant MXene-decorated polyester textiles with outstanding electromagnetic interference shielding and joule heating performances. *Adv. Funct. Mater.* **2019**, *29*, 1806819. [CrossRef]
121. Park, T.H.; Yu, S.; Koo, M.; Kim, H.; Kim, E.H.; Park, J.-E.; Ok, B.; Kim, B.; Noh, S.H.; Park, C. Shape-adaptable 2D titanium carbide (MXene) heater. *ACS Nano* **2019**, *13*, 6835–6844. [CrossRef]
122. Zhao, X.; Peng, L.-M.; Tang, C.-Y.; Pu, J.-H.; Zha, X.-J.; Ke, K.; Bao, R.-Y.; Yang, M.-B.; Yang, W. All-weather-available, continuous steam generation based on the synergistic photo-thermal and electro-thermal conversion by MXene-based aerogels. *Mater. Horiz.* **2020**, *7*, 855–865. [CrossRef]
123. Mazhar, S.; Qarni, A.A.; Haq, Y.U.; Haq, Z.U.; Murtaza, I. Promising PVC/MXene based flexible thin film nanocomposites with excellent dielectric, thermal and mechanical properties. *Ceram. Int.* **2020**, *46*, 12593–12605. [CrossRef]
124. Borysiuk, V.; Mochalin, V.N. Thermal stability of two-dimensional titanium carbides $Ti_{n+1}C_n$ (MXenes) from classical molecular dynamics simulations. *MRS Commun.* **2019**, *9*, 203–208. [CrossRef]
125. Jin, X.; Wang, J.; Dai, L.; Liu, X.; Li, L.; Yang, Y.; Cao, Y.; Wang, W.; Wu, H.; Guo, S. Flame-retardant poly (vinyl alcohol)/MXene multilayered films with outstanding electromagnetic interference shielding and thermal conductive performances. *Chem. Eng. J.* **2020**, *380*, 122475. [CrossRef]
126. Zhang, P.; Liao, Q.; Yao, H.; Huang, Y.; Cheng, H.; Qu, L. Direct solar steam generation system for clean water production. *Energy Storage Mater.* **2019**, *18*, 429–446. [CrossRef]
127. Zhao, X.; Zha, X.-J.; Pu, J.-H.; Bai, L.; Bao, R.-Y.; Liu, Z.-Y.; Yang, M.-B.; Yang, W. Macroporous three-dimensional MXene architectures for highly efficient solar steam generation. *J. Mater. Chem. A* **2019**, *7*, 10446–10455. [CrossRef]
128. Zha, X.-J.; Zhao, X.; Pu, J.-H.; Tang, L.-S.; Ke, K.; Bao, R.-Y.; Bai, L.; Liu, Z.-Y.; Yang, M.-B.; Yang, W. Macroporous three-dimensional MXene architectures for highly efficient solar steam generation. *J. Mater. Chem. A ACS Appl. Mater. Interfaces* **2019**, *11*, 36589–36597. [CrossRef]
129. Zhao, J.; Yang, Y.; Yang, C.; Tian, Y.; Han, Y.; Liu, J.; Yin, X.; Que, W. A hydrophobic surface enabled salt-blocking 2D Ti_3C_2 MXene membrane for efficient and stable solar desalination. *J. Mater. Chem. A* **2018**, *6*, 16196–16204. [CrossRef]